

## Aerosol species concentrations and source apportionment of ammonia at Rocky Mountain National Park

William C. Malm , Bret A. Schichtel , Michael G. Barna , Kristi A. Gebhart , Marco A. Rodriguez , Jeffrey L. Collett Jr. , Christian M. Carrico , Katherine B. Benedict , Anthony J. Prenni & Sonia M. Kreidenweis

To cite this article: William C. Malm , Bret A. Schichtel , Michael G. Barna , Kristi A. Gebhart , Marco A. Rodriguez , Jeffrey L. Collett Jr. , Christian M. Carrico , Katherine B. Benedict , Anthony J. Prenni & Sonia M. Kreidenweis (2013) Aerosol species concentrations and source apportionment of ammonia at Rocky Mountain National Park, Journal of the Air & Waste Management Association, 63:11, 1245-1263, DOI: [10.1080/10962247.2013.804466](https://doi.org/10.1080/10962247.2013.804466)

To link to this article: <http://dx.doi.org/10.1080/10962247.2013.804466>



Accepted author version posted online: 06 Jun 2013.



Submit your article to this journal [↗](#)



Article views: 204



View related articles [↗](#)



Citing articles: 4 View citing articles [↗](#)

# Aerosol species concentrations and source apportionment of ammonia at Rocky Mountain National Park

William C. Malm,<sup>1,\*</sup> Bret A. Schichtel,<sup>2</sup> Michael G. Barna,<sup>2</sup> Kristi A. Gebhart,<sup>2</sup> Marco A. Rodriguez,<sup>3</sup> Jeffrey L. Collett, Jr.,<sup>4</sup> Christian M. Carrico,<sup>3</sup> Katherine B. Benedict,<sup>4</sup> Anthony J. Prenni,<sup>4</sup> and Sonia M. Kreidenweis<sup>4</sup>

<sup>1</sup>Cooperative Institute for Research in the Atmosphere, Colorado State University, Fort Collins, Colorado, USA

<sup>2</sup>National Park Service, Cooperative Institute for Research in the Atmosphere, Colorado State University, Fort Collins, Colorado, USA

<sup>3</sup>AECOM, Fort Collins, Colorado, USA

<sup>4</sup>Department of Atmospheric Science, Colorado State University, Fort Collins, Colorado, USA

\*Please address correspondence to: William C. Malm, Cooperative Institute for Research in the Atmosphere (CIRA), Colorado State University, 1375 Campus Delivery, Fort Collins, CO 80523-1375, USA; e-mail: malm@cira.colostate.edu

---

*Changes in ecosystem function at Rocky Mountain National Park (RMNP) are occurring because of emissions of nitrogen and sulfate species along the Front Range of the Colorado Rocky Mountains, as well as sources farther east and west. The nitrogen compounds include both oxidized and reduced nitrogen. A year-long monitoring program of various oxidized and reduced nitrogen species was initiated to better understand their origins as well as the complex chemistry occurring during transport from source to receptor. Specifically, the goals of the study were to characterize the atmospheric concentrations of nitrogen species in gaseous, particulate, and aqueous phases (precipitation and clouds) along the east and west sides of the Continental Divide; identify the relative contributions to atmospheric nitrogen species in RMNP from within and outside of the state of Colorado; identify the relative contributions to atmospheric nitrogen species in RMNP from emission sources along the Colorado Front Range versus other areas within Colorado; and identify the relative contributions to atmospheric nitrogen species from mobile sources, agricultural activities, and large and small point sources within the state of Colorado. Measured ammonia concentrations are combined with modeled releases of conservative tracers from ammonia source regions around the United States to apportion ammonia to its respective sources, using receptor modeling tools.*

*Implications:* Increased deposition of nitrogen in RMNP has been demonstrated to contribute to a number of important ecosystem changes. The rate of deposition of nitrogen compounds in RMNP has crossed a crucial threshold called the “critical load.” This means that changes are occurring to park ecosystems and that these changes may soon reach a point where they are difficult or impossible to reverse. Several key issues need attention to develop an effective strategy for protecting park resources from adverse impacts of elevated nitrogen deposition. These include determining the importance of previously unquantified nitrogen inputs within the park and identification of important nitrogen sources and transport pathways.

---

## Introduction

Atmospheric nitrogen and sulfur species can cause a number of deleterious effects, including visibility impairment and changes in ecosystem function and surface water chemistry from atmospheric deposition. Within Rocky Mountain National Park (RMNP), an area of particular interest, wet deposition of inorganic nitrogen (nitrate and ammonium) currently contributes approximately 3 kg/ha/yr to total nitrogen input (Baron et al., 2011). Dry deposition of nitric acid (HNO<sub>3</sub>) and particulate nitrate and ammonium (NH<sub>4</sub><sup>+</sup>) increases total measured nitrogen deposition to approximately 4 kg/ha/yr. These current nitrogen deposition flux values appear to represent approximately a 20-fold increase above preindustrial values for the western United States (Galloway et al., 1982, 1995; Hedin et al., 1995).

Increased deposition of nitrogen in RMNP has been demonstrated to contribute to a number of important ecosystem changes (for a review see Blett and Morris, 2004). Among these are changes in the chemistry of old-growth Engelmann spruce forests (Rueth and Baron, 2002), shifts in population of lake diatoms (Baron et al., 2000), excess nitrogen leakage into lakes and streams at certain times of the year (Campbell et al., 2000), and alterations in biogeochemical cycling associated with increased microbial activity in high elevation soils and talus (Campbell et al., 2000, 2002; Rueth and Baron, 2002). Several of these effects have been noted mainly on the east side of the Continental Divide that runs through RMNP. Nitrogen deposition levels have also been determined to be higher on the eastern slope of the park (Burns, 2003). Nitrate wet deposition has increased by approximately 10–20%, and ammonium wet deposition has increased by about 50% (Lehmann et al., 2005).

The Rocky Mountain Atmospheric Nitrogen and Sulfur (RoMANS) study was initiated to better understand the origins and physical/chemical and optical characteristics of nitrogen species, as well as the complex chemistry occurring during transport from source to receptor. Assessing changes in ambient concentrations of aerosol species and wet deposition as a function of changing ammonia and nitrogen oxide concentrations is dependent on a number of chemical and physical mechanisms, as well as meteorological conditions and transport characteristics. For example, ammonia will increase particle mass by reacting with acidic sulfate aerosols, nitric acid, and organic acids. With respect to the reaction of ammonia with nitric acid, the equilibrium between these species and the reaction product, ammonium nitrate, is temperature dependent and can go from predominantly gases to particles with the diurnal shifts in temperature. The condensation of ammonia onto particles is also dependent on the acidity of the particles and ambient relative humidity. These reactions do not necessarily take place at or near the source of ammonia, but over the transport pathways from source to receptor (Seinfeld and Pandis, 1998). Actually, sources of nitric acid, acidic sulfates, and organic acids are not likely to be associated with ammonia sources.

Increases in ammonia emissions will tend to increase and change the composition of particulate matter (PM) mass concentrations. Regardless of the chemical form and phase of the nitrogen, it will ultimately be deposited onto terrestrial or aquatic surfaces, but where these species are deposited does depend on the chemical form and phase of the nitrogen. For example, gaseous ammonia has higher deposition rates and will deposit closer to the sources, while ammoniated particulates can be transported hundreds of kilometers before deposition.

As part of the study, a monitoring program was initiated for one year, starting in November 2008. The monitoring program

consisted of intensive, high time resolution measurements of particles, gas, wet deposition, and meteorology at a core site, subsequently referred to as the receptor site, near RMNP. This paper includes a discussion of aerosol species concentrations collected at RMNP, and because little effort has been focused on understanding sources responsible for elevated ambient ammonia concentrations in RMNP, an apportionment of measured ammonia concentrations to sources of ammonia using hybrid receptor modeling techniques is presented.

## Measurements

A 12-month intensive monitoring program was conducted, starting on November 11, 2008. A summary of the measurements is included in Table 1. Gas-phase measurements were made continuously and in real time, with 1-min averaged data. Instrumentation was housed in a temperature-controlled ( $25 \pm 5^\circ\text{C}$ ) shelter (National Park Service air quality shelter), collocated with the existing Interagency Monitoring of Protected Visual Environments (IMPROVE) (Hand et al., 2011) and Clean Air Status and Trends Network (CASTNET) (CASTNET, 2010) sites near the eastern boundary of RMNP.

The configuration of the gas-phase instrument is shown in Figure 1. Measurements of nitric oxide (NO) and  $\text{NO}_y$  were made using a Teledyne-API, Inc. (M200EU),  $\text{NO}_y$  chemiluminescence instrument (Fontijn et al., 1970; Fehsenfeld et al., 1987; Williams et al., 1998; Demerjian, 2000; Parrish and Fehsenfeld, 2000), with a detection limit of 50 ppt. For these studies, the converter temperature was set to  $285^\circ\text{C}$  (instead of  $315^\circ\text{C}$ ) to minimize potential  $\text{NH}_3$  interference (Williams et al., 1998), as determined from laboratory tests. Ambient air was sampled through a Teflon sampling line, located  $\sim 4$  m above ground level; residence time in the sampling line was  $\sim 8$  sec.

**Table 1.** Measurements at the core sites

| Measurement  | Instrument  | Time resolution | Notes  |
|--|---|-----------------|--|
| $\text{PM}_{2.5}$ inorganic ions and gases   | Annular denuder/filter-pack sampler   | 24 hr           | $\text{Cl}^-$ , $\text{NO}_2^-$ , $\text{NO}_3^-$ , $\text{SO}_4^{2-}$ , $\text{Na}^+$ , $\text{K}^+$ , $\text{NH}_4^+$ , $\text{Mg}^{2+}$ , $\text{Ca}^{2+}$ , $\text{HNO}_3$ , $\text{NH}_3$ |
| $\text{PM}_{2.5}$ inorganic ions   | Particle-into-liquid sampler (PILS)–IC  | 15 min          | $\text{Cl}^-$ , $\text{NO}_2^-$ , $\text{NO}_3^-$ , $\text{SO}_4^{2-}$ , $\text{Na}^+$ , $\text{K}^+$ , $\text{NH}_4^+$ , $\text{Mg}^{2+}$ , $\text{Ca}^{2+}$                                  |
| $\text{PM}_{2.5}$ mass, ions, elements, H, and OC/EC   | IMPROVE sampler   | 24 hr           | Components per IMPROVE protocol  |
| $\text{PM}_{10}$ mass  | IMPROVE sampler   | 24 hr           | Components per IMPROVE protocol  |
| $\text{NO}_x$ , $\text{NO}_y$ , $\text{HNO}_3$ , $\text{TN}_x$ , $\text{NH}_{x,\text{gas}}$ , CO | Various continuous gas monitors   | 1 min           | An estimate of reduced nitrogen other than ammonia.  |
| Meteorological parameters  | Met station   | 2 min           | T, RH, WD, WS, Precip, SR,BP   |
| Particle size distributions  | Differential mobility particle sizing (DMPS) system, optical particle counter (OPC), aerodynamic particle sizer (APS) | 15 min          | 0.05–10 $\mu\text{m}$ diameter   |
| Particle light scattering  | Nephelometer  | 2 min           | Ambient $\text{PM}_{2.5}$ aerosol  |

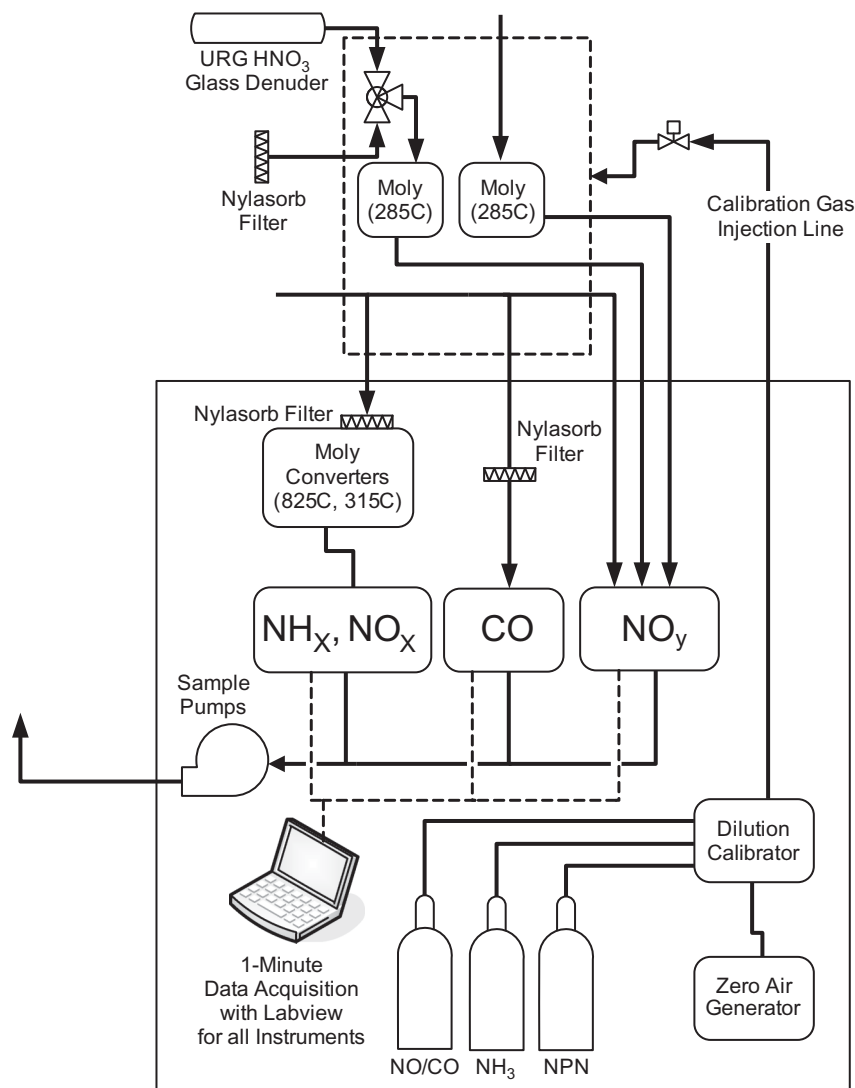


**Figure 1.** Schematic of the physical configuration of gaseous monitoring system.

The inlet to the NO<sub>y</sub> instrument was modified to allow for two additional measurement channels. For the first, ambient air passed through an inline glass denuder (URG, Inc., model URG-2000-30x242-3CSS) coated with NaCl solution, removing gas-phase HNO<sub>3</sub> (Bai and Wen, 2000) prior to measurement with the NO<sub>y</sub> instrument. The difference between this measurement and total NO<sub>y</sub> provided a measure of HNO<sub>3</sub> (g). The inlet was programmed to switch between this channel and a second channel on an hourly basis. For the second channel, ambient air passed through an upstream filter (Pall Corp., Nylasorb, 1 μm pore), which efficiently removed particulate material and HNO<sub>3</sub> from the sample. This measurement, in conjunction with total NO<sub>y</sub> and HNO<sub>3</sub> (g), provided an estimate of particulate nitrate concentrations. After passing through the modified inlet, these two additional channels, termed NO' (HNO<sub>3</sub> or particulate), followed the same path as the NO<sub>y</sub> measurement.

A second chemiluminescence instrument (Teledyne-API, Inc., model 201E) was utilized to determine concentrations for additional nitrogen species (NO<sub>x</sub>, NO<sub>2</sub>, NH<sub>3</sub>, a redundant measurement of NO, and total gas-phase nitrogen species). This

three-channel instrument utilized an upstream nylon membrane filter for all channels and at all times to remove particulate material and HNO<sub>3</sub>. NO<sub>x</sub> measurements via chemiluminescence likely measure some NO<sub>y</sub> compounds other than NO<sub>2</sub> + NO, as the conversion is nonspecific to NO<sub>2</sub> (Demerjian, 2000; Parrish and Fehsenfeld, 2000; Dunlea et al., 2007). For NH<sub>3</sub> and total gas-phase nitrogen species, a model 501NH converter was used upstream of the NO<sub>x</sub> analyzer. Laboratory testing demonstrated that other reduced nitrogen species are also effectively converted to NO in this converter. Ambient air was sampled at the same point in space as the NO<sub>y</sub> instrument through an ~4-m-long, 1/4-inch Teflon sampling line. To improve low-level sensitivity, the NH<sub>3</sub>/NO<sub>x</sub> instrument was retrofitted with a gold-plated reaction cell and pumped with an external high vacuum pump.

A trace-level CO analyzer (Teledyne-API, Inc., model 300EU) was also operated, with a detection limit of <20 ppb. Calibrations for most instruments were performed on an almost daily basis. For NH<sub>3</sub>, a calibration was done before, once during, and after the study.

Measurements for the RMNP core site also included detailed observations of fine ( $PM_{2.5}$ ) particle composition and coarse ( $PM_{10}$ ) particle composition, ion size distributions, trace gas concentrations, wet deposition, particle size distributions, particle light scattering, and meteorology. Both time-integrated and high time resolution (at least hourly) measurements were made for nearly all measurement parameters at the core site (Malm et al., 2005).

## The Data Set

### Species concentrations

Table 2 presents an overall statistical data summary, as well as by season, for a number of parameters measured during the field campaign.  $PM_1$  refers to fine particle mass less than 1.0  $\mu m$ , derived from the tandem differential mobility analyzer (TDMA) particle size distribution measurements that were made every 15 min. An average particle density of 1.7  $g/m^3$  was assumed (Malm et al., 2005). The data were averaged to 24 hr, and it is the 24-hr statistics that are presented in Table 2.  $SO_4$ ,  $NO_3$ , and  $NH_4$  are the sulfate, nitrate, and ammonium ion concentrations, respectively, collected over a 24-hr period with the URG sampler, while  $NH_{3,urg}$  is the URG denuder measurement of ammonia gas.  $NH_4B$  is the ammonium concentration collected on a backup filter, which corresponds to the volatilized ammonia gas from the nylon front filter. It is the sum of  $NH_4$  and  $NH_4B$  that corresponds to total particle ammonium.  $NH_{x,gas}$ ,  $NO_x$ ,  $NO_y$ , and  $HNO_3$  are the statistical summaries of the 24-hr average  $NH_{x,gas}$ , ( $NO + NO_2$ ),  $NO_y$ —an estimate of all oxidized nitrogen species—and gaseous nitric acid, all derived from the chemiluminescent measurement.  $NH_{x,gas}$  refers to  $NH_3$  + other reduced nitrogen species. Particulate organic matter (POM) is estimated by differencing  $PM_1$  and  $SO_4 + NO_3$  interpreted as being in the fully ammoniated state. Because the TDMA data from which  $PM_1$  and therefore POM are derived have significant periods in which a 15-min sampling interval is missing, the number of valid POM data points reported in Table 2 is often less than for the gaseous species. For the sake of comparison, only statistical summaries for the URG ion data that correspond in time to the POM data are reported. The units of concentration for mass species are in micrograms per cubic meter ( $\mu g/m^3$ ), while those for gas species are in parts per billion.

As a quality control check, URG sulfate and nitrate ion concentrations were compared to those measured in the IMPROVE program. Concurrently measured sulfate over the same time period showed good agreement, with a comparative  $R^2 = 0.87$  and an ordinary least squares (OLS)-derived slope of a scatterplot between the two variables of  $0.98 \pm 0.02$ .

### Temporal variability of aerosol species

The data in Table 2 are further summarized in Figures 2a and 2b. Figure 2a shows the particulate species average concentrations as an overall average and averages for each season, while Figure 2b presents the same information but for selected measured gas species. On the average, POM makes up about 56% of the fine mass, with sulfates, nitrates, and ammonium contributing on the order of 23%, 8%, and 13%, respectively. All species

show seasonal variability, with winter having the lowest concentrations and spring and summer the higher concentrations. PM is highest during the summer at 2.54  $\mu g/m^3$  and lowest during the winter at 0.46  $\mu g/m^3$ . POM is also highest during the summer months, making up about 70% of PM. On the other hand, sulfates, the second largest contributor to PM, are highest during the fall, when they make up approximately 44% of PM.

While all particle species show significant variability,  $NO_x$ ,  $NO_y$ , and  $HNO_3$  gas species show little change over the seasons, although winter concentrations are somewhat lower than other seasons.  $HNO_3$  makes up about 12% of  $NO_y$  on the average. Also shown in Figure 2 are the average seasonal  $NH_{x,gas}$  and  $NH_3$  concentrations. Remember that  $NH_{x,gas}$  is measured with the modified chemiluminescence instrument, while  $NH_3$  was estimated using a URG sampler fitted with an  $NH_3$  gas denuder.  $NH_{x,gas}$  is a semicontinuous measurement averaged to 24 hr, while the URG is a 24-hr measurement. Both variables have significant seasonal and similar relative cycles, with winter having the lowest concentrations, summer the highest, and spring and fall intermediate concentrations. However,  $NH_{x,gas}$  is about four times greater than  $NH_3$ , implying that there are significant levels of reduced nitrogen gases other than  $NH_3$ . This topic is discussed at some length later.

Figure 3 shows a temporal plot of 24-hr average values of  $NH_{x,gas}$ ,  $NO_y$ , and  $HNO_3$ , three variables that are representative of the temporal variability of all measured gaseous species.  $NO_y$  and  $NO_x$  show very similar temporal variability. Shorter time scale or diurnal variability of gaseous species is discussed in the next section.  $NH_{x,gas}$  exhibits highest concentrations during summer time periods, with higher concentration episodes lasting as long as a week, while during other times of the year episodes are of shorter duration.  $NO_x$  and  $NO_y$  species are episodic on a shorter time scale than  $NH_{x,gas}$ , and during the summer time frame, the variability between high and low concentrations is significantly less than during other months. As expected,  $HNO_3$  is about a factor of 10 lower than  $NO_y$  or  $NO_x$ , with summer months being less episodic than other seasons, and is lower during winter and summer months compared to spring and fall.

### Diurnal variability

The summer diurnal variability of various aerosol species was explored by first grouping all hourly observations for the summer time period into separate data sets. The median and 10th, 25th, 75th, and 90th percentile concentrations of each group corresponding to each hour of the day were then calculated. These percentile values are presented as box-and-whisker plots for  $PM_1$ ,  $NH_{x,gas}$ ,  $NO_y$ ,  $NO_x$ , temperature, and wind direction in Figure 4. Gaps in the data series correspond to calibration periods. Wind direction was measured on a 10-m tower at the core site in RMNP.

In each box-and-whisker plot there are maximum and minimum median values. The median difference ratio (MDR) is defined as the ratio of the difference between the maximum and minimum median values divided by the maximum median value. Figure 5 is a plot of the median difference ratio for each species. All species exhibit significant diurnal patterns, although the hours at which the maximum and minimum occur are not the same. In general, the concentrations increase uniformly from about 6:00 a.m. (all times MST) to about 3:00 p.m. and then

**Table 2.** Statistical summary of selected PM and gas species concentrations for the entire year as well as seasonally

| Variable                                 | Mean | Std dev | Minimum | Maximum | Valid |
|--|------|---------|---------|---------|-------|
| <b>All</b>                               |      |         |         |         |       |
| PM <sub>1</sub> (μg/m <sup>3</sup> )     | 1.83 | 1.88    | 0.13    | 20.26   | 185   |
| SO <sub>4</sub> (μg/m <sup>3</sup> )     | 0.42 | 0.28    | 0.06    | 2.42    | 185   |
| NO <sub>3</sub> (μg/m <sup>3</sup> )     | 0.15 | 0.18    | 0.00    | 1.48    | 185   |
| POM (μg/m <sup>3</sup> )                 | 1.02 | 1.61    | 0.00    | 17.54   | 185   |
| NH <sub>4</sub> (μg/m <sup>3</sup> )     | 0.13 | 0.14    | 0.00    | 1.01    | 185   |
| NH <sub>4</sub> B (μg/m <sup>3</sup> )   | 0.10 | 0.10    | 0.00    | 0.73    | 185   |
| NH <sub>x,gas</sub> (ppb)                | 2.63 | 1.54    | 0.17    | 6.97    | 336   |
| NH <sub>3</sub> URG (ppb)                | 0.45 | 0.34    | 0.00    | 2.51    | 340   |
| NO <sub>x</sub> (ppb)                    | 1.32 | 0.92    | 0.13    | 6.85    | 339   |
| NO <sub>y</sub> (ppb)                    | 1.53 | 1.10    | 0.13    | 7.64    | 339   |
| HNO <sub>3</sub> (ppb)                   | 0.14 | 0.13    | 0.00    | 0.80    | 356   |
| <b>Winter</b>                            |      |         |         |         |       |
| WPM <sub>1</sub> (μg/m <sup>3</sup> )    | 0.46 | 0.60    | 0.13    | 3.03    | 21    |
| WSO <sub>4</sub> (μg/m <sup>3</sup> )    | 0.19 | 0.14    | 0.06    | 0.70    | 21    |
| WNO <sub>3</sub> (μg/m <sup>3</sup> )    | 0.08 | 0.16    | 0.01    | 0.78    | 21    |
| WPOM (μg/m <sup>3</sup> )                | 0.08 | 0.17    | 0.00    | 0.80    | 21    |
| WNH <sub>4</sub> (μg/m <sup>3</sup> )    | 0.05 | 0.07    | 0.00    | 0.32    | 21    |
| WNH <sub>4</sub> B (μg/m <sup>3</sup> )  | 0.05 | 0.09    | 0.00    | 0.43    | 21    |
| NH <sub>x,gas</sub> (ppb)                | 1.51 | 0.69    | 0.17    | 4.28    | 81    |
| NH <sub>3</sub> URG (ppb)                | 0.16 | 0.17    | 0.00    | 0.90    | 88    |
| NO <sub>x</sub> (ppb)                    | 1.00 | 0.95    | 0.16    | 4.22    | 82    |
| NO <sub>y</sub> (ppb)                    | 1.14 | 1.17    | 0.16    | 5.44    | 82    |
| HNO <sub>3</sub> (ppb)                   | 0.08 | 0.11    | 0.00    | 0.58    | 90    |
| <b>Spring</b>                            |      |         |         |         |       |
| SPPM <sub>1</sub> (μg/m <sup>3</sup> )   | 1.35 | 0.49    | 0.56    | 2.70    | 20    |
| SPSO <sub>4</sub> (μg/m <sup>3</sup> )   | 0.50 | 0.22    | 0.17    | 0.91    | 20    |
| SPNO <sub>3</sub> (μg/m <sup>3</sup> )   | 0.20 | 0.18    | 0.03    | 0.74    | 20    |
| SPPOM (μg/m <sup>3</sup> )               | 0.33 | 0.23    | 0.00    | 0.78    | 20    |
| SPNH <sub>4</sub> (μg/m <sup>3</sup> )   | 0.16 | 0.14    | 0.00    | 0.43    | 20    |
| SPNH <sub>4</sub> B (μg/m <sup>3</sup> ) | 0.16 | 0.10    | 0.05    | 0.39    | 20    |
| NH <sub>x,gas</sub> (ppb)                | 2.84 | 1.25    | 0.70    | 6.52    | 90    |
| NH <sub>3</sub> URG (ppb)                | 0.61 | 0.45    | 0.00    | 2.55    | 91    |
| NO <sub>x</sub> (ppb)                    | 1.39 | 0.98    | 0.38    | 4.71    | 90    |
| NO <sub>y</sub> (ppb)                    | 1.65 | 1.17    | 0.38    | 6.07    | 92    |
| HNO <sub>3</sub> (ppb)                   | 0.18 | 0.14    | 0.00    | 0.80    | 93    |
| <b>Summer</b>                            |      |         |         |         |       |
| SPM <sub>1</sub> (μg/m <sup>3</sup> )    | 2.54 | 2.59    | 0.40    | 20.26   | 68    |
| SSO <sub>4</sub> (μg/m <sup>3</sup> )    | 0.45 | 0.14    | 0.13    | 0.96    | 68    |
| SNO <sub>3</sub> (μg/m <sup>3</sup> )    | 0.13 | 0.15    | 0.00    | 1.08    | 68    |
| SPOM (μg/m <sup>3</sup> )                | 1.74 | 2.29    | 0.09    | 17.54   | 68    |
| SNH <sub>4</sub> (μg/m <sup>3</sup> )    | 0.11 | 0.08    | 0.00    | 0.50    | 68    |
| SNH <sub>4</sub> B (μg/m <sup>3</sup> )  | 0.12 | 0.06    | 0.00    | 0.30    | 68    |
| NH <sub>x,gas</sub> (ppb)                | 4.21 | 1.33    | 1.58    | 6.97    | 84    |
| NH <sub>3</sub> URG (ppb)                | 1.05 | 3.22    | 0.00    | 23.83   | 92    |
| NO <sub>x</sub> (ppb)                    | 1.36 | 0.50    | 0.48    | 2.79    | 86    |
| NO <sub>y</sub> (ppb)                    | 1.62 | 0.64    | 0.59    | 3.32    | 84    |
| HNO <sub>3</sub> (ppb)                   | 0.18 | 0.12    | 0.00    | 0.65    | 92    |
| <b>Fall</b>                              |      |         |         |         |       |
| FPM <sub>1</sub> (μg/m <sup>3</sup> )    | 1.65 | 1.09    | 0.29    | 4.76    | 61    |
| FSO <sub>4</sub> (μg/m <sup>3</sup> )    | 0.47 | 0.39    | 0.09    | 2.42    | 61    |
| FNO <sub>3</sub> (μg/m <sup>3</sup> )    | 0.18 | 0.21    | 0.00    | 1.48    | 61    |
| FPOM (μg/m <sup>3</sup> )                | 0.72 | 0.75    | 0.05    | 3.69    | 61    |

(Continued)

Table 2. (Cont.)

| Variable                                | Mean | Std dev | Minimum | Maximum | Valid |
|---|------|---------|---------|---------|-------|
| FNH <sub>4</sub> (μg/m <sup>3</sup> )   | 0.18 | 0.20    | 0.01    | 1.01    | 61    |
| FNH <sub>4</sub> B (μg/m <sup>3</sup> ) | 0.09 | 0.12    | 0.00    | 0.73    | 61    |
| NH <sub>x,gas</sub> (ppb)               | 1.99 | 1.16    | 0.53    | 5.56    | 72    |
| NH <sub>3</sub> URG (ppb)               | 0.36 | 0.42    | 0.00    | 2.50    | 71    |
| NO <sub>x</sub> (ppb)                   | 1.49 | 0.92    | 0.34    | 4.70    | 72    |
| NO <sub>y</sub> (ppb)                   | 1.71 | 1.07    | 0.36    | 5.06    | 72    |
| HNO <sub>3</sub> (ppb)                  | 0.12 | 0.11    | 0.00    | 0.52    | 72    |

Notes: The data were first averaged to 24 hr and then averaged for the whole year and seasonally. Winter = December, January, February; Spring = March, April, May; Summer = June, July, August; Fall = September, October, November.

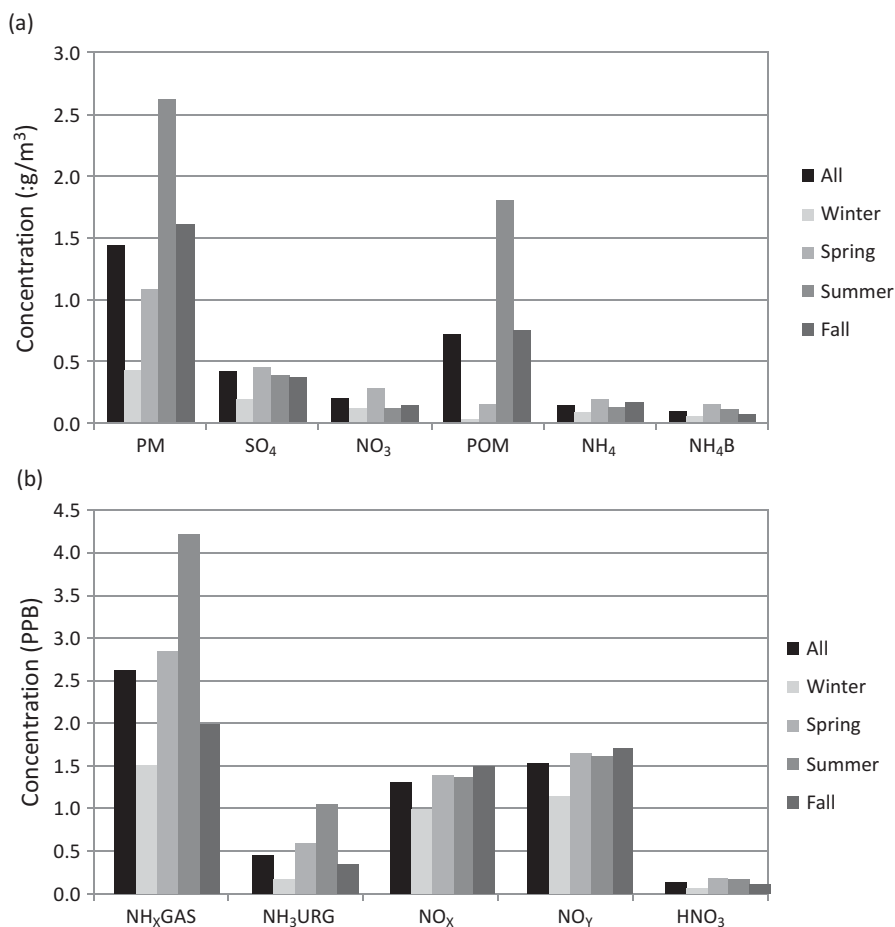


**Figure 2.** (a) Bar plot of measured concentrations of PM<sub>1.0</sub> and the species contributing to PM<sub>1.0</sub> plotted as an overall average and for each season. NH<sub>4</sub>B is a measure of the NH<sub>4</sub> volatilized as NH<sub>3</sub> from the NH<sub>3</sub>NO<sub>3</sub> collected on the Nylasorb filter. (b) Bar plot of selected gas species plotted as an overall average and as seasonal averages. Concentrations of particle mass are expressed in μg/m<sup>3</sup>, while gas concentrations are presented in ppb.

remain elevated throughout the early evening hours. PM<sub>1</sub> reaches its average maximum median value at 6:00 p.m. and its minimum median value at 8:00 a.m.

The increase in NH<sub>x,gas</sub> concentrations from an 8:00 a.m. morning low to a secondary maximum at about 11:00 a.m. is quite abrupt. Concentrations then decrease and again increase to reach their maximum level at about 3:00 p.m., decreasing from then until about midnight.

NO<sub>x</sub> and NO<sub>y</sub> concentrations have afternoon maximums occurring at about 6:00 p.m. and morning minimums at between 10:00 a.m. and 12:00 p.m. Temperature, of course, also has a strong diurnal variation, with morning minimums occurring from 12:00 to 6:00 a.m. and afternoon maximums around noon.

During the evening hours, winds are generally from the north-west, while during daytime from about 7:00 a.m. to 6:00 p.m.

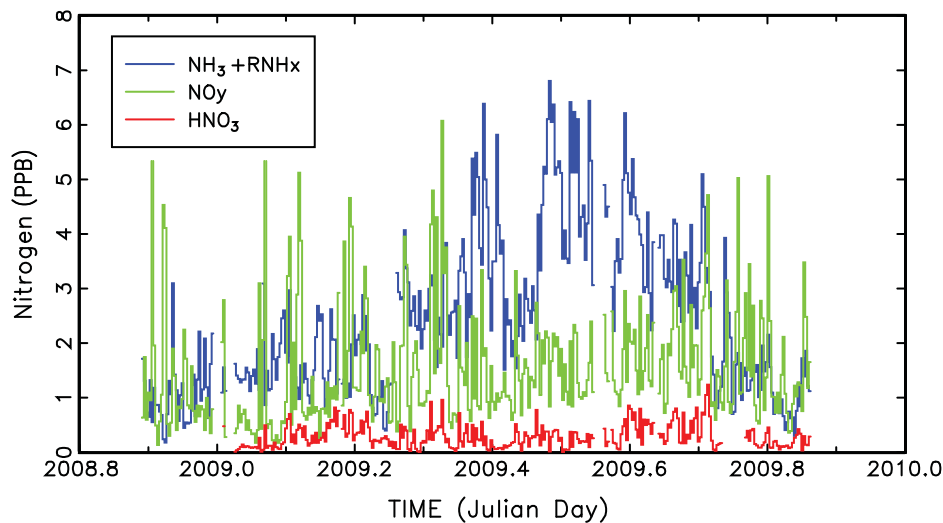


Figure 3. Temporal plot of chemiluminescence measured concentrations of  $\text{NH}_{x,\text{gas}}$ ,  $\text{NO}_y$ , and  $\text{HNO}_3$ .

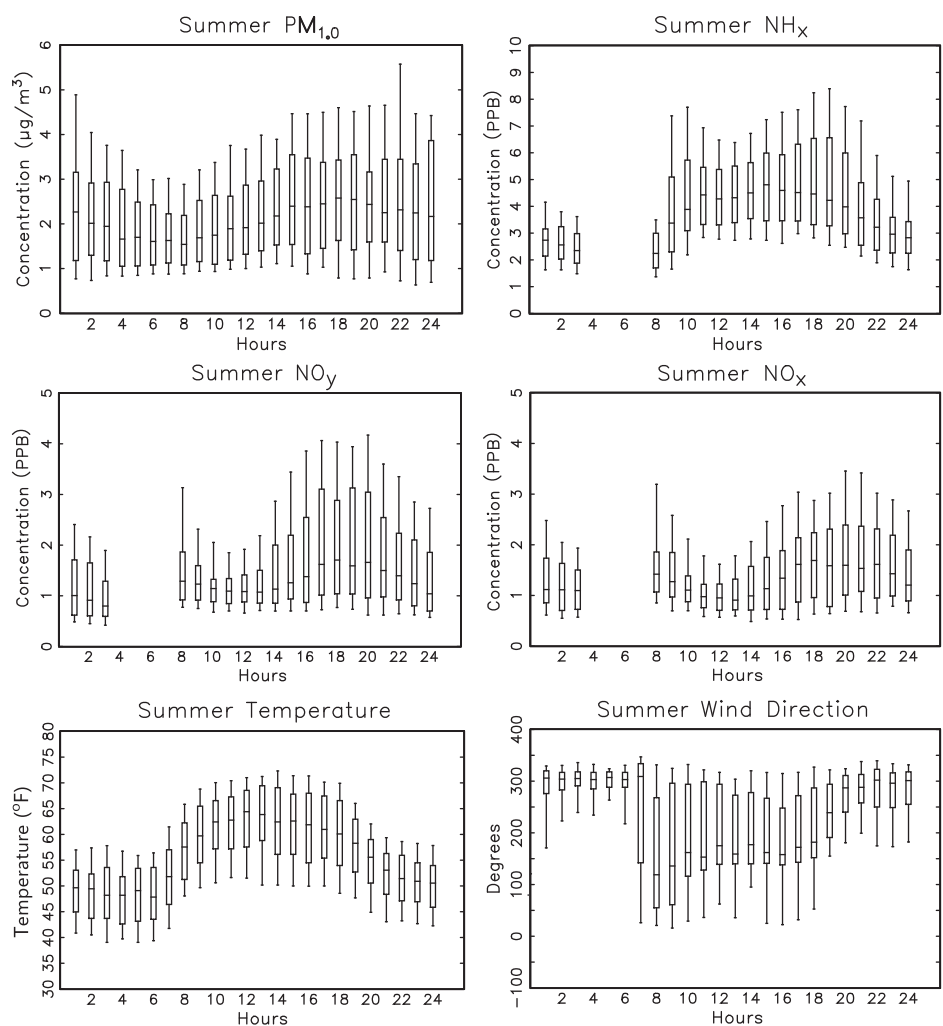
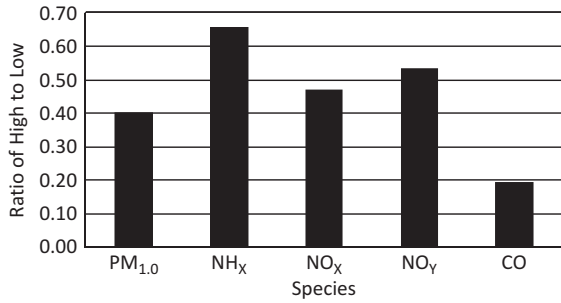


Figure 4. Box-and-whisker plots of measured hourly  $\text{PM}_{1.0}$ ,  $\text{NH}_3$ ,  $\text{NO}_y$ ,  $\text{NO}_x$ , temperature, and wind direction for the summer time period with the median and 10th, 25th, 75th, and 90th percentiles shown.



**Figure 5.** Median difference ratio for each species shown in Figure 4. The median difference ratio is defined as the ratio of the difference between the hourly maximum and minimum median values divided by the hourly maximum median value.

winds shift to southeasterly transport, suggesting transport from the Front Range to the receptor site.

Figure 5 shows that NH<sub>3</sub> has the highest or greatest median difference ratio of about 0.65, while NO<sub>x</sub> and NO<sub>y</sub> are also very high at about 0.50. The median difference ratio for PM<sub>1</sub> is lower but still high at 0.40.

### Examples of daily variability of NH<sub>x,gas</sub>, NO<sub>y</sub>, NO<sub>x</sub>, and PM<sub>1,0</sub>

Figure 6 is a plot of hourly average species concentrations for various Julian days. Concentrations are in PPB and time is expressed in astronomical time. While Figure 4 shows average

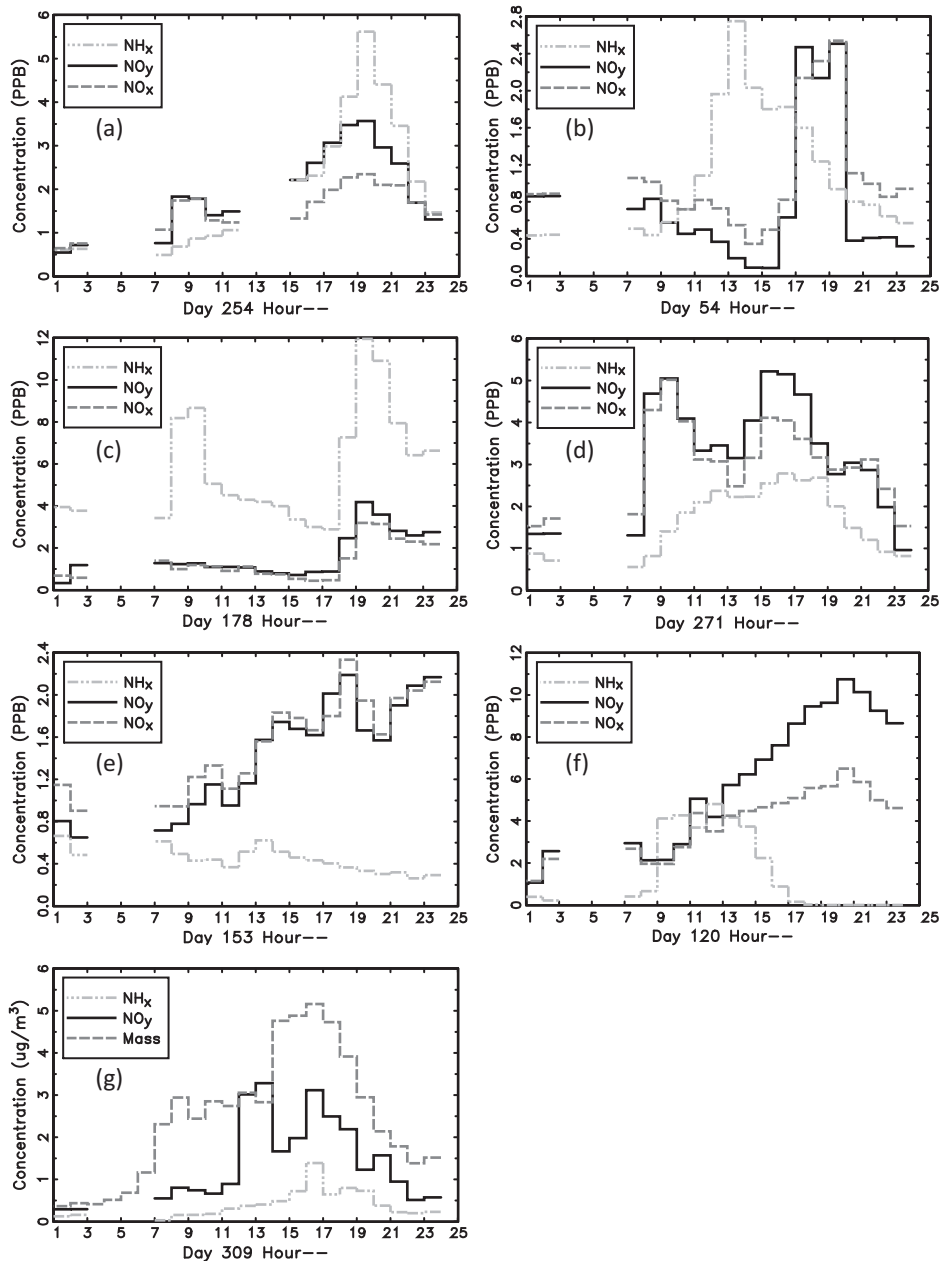


**Figure 6.** (a)–(f) Hourly average species concentrations of measured NH<sub>x,gas</sub>, NO<sub>y</sub>, and NO<sub>x</sub> for various Julian days; (g) temporal variability of NH<sub>x,gas</sub>, NO<sub>y</sub>, and PM<sub>1</sub> for Julian Day 309. Concentrations are in ppb and  $\mu\text{g}/\text{m}^3$ , and time is expressed as Julian Day and hours of the day in international time units.

diurnal variability of four species, Figure 6 shows examples of specific patterns of diurnal variability of  $\text{NH}_{x,\text{gas}}$ ,  $\text{NO}_x$ , and  $\text{NO}_y$ . Figure 6a shows an example in which all three species have similar diurnal patterns, with all species reaching an afternoon/evening maximum at 7:00 p.m. All species having the same diurnal pattern suggests similar transport pathways and possibly similar source regions.

Figures 6b and 6c show more typical patterns in which  $\text{NH}_{x,\text{gas}}$  concentrations peak before  $\text{NO}_x$  and  $\text{NO}_y$  concentrations. Figure 6b shows an example in which the temporal variability of  $\text{NH}_{x,\text{gas}}$  varies independently from  $\text{NO}_x$  and  $\text{NO}_y$ , with  $\text{NH}_{x,\text{gas}}$  peaking about 4 hr before  $\text{NO}_x$  and  $\text{NO}_y$ , suggesting different source regions. Figure 6c shows an interesting example of an  $\text{NH}_{x,\text{gas}}$  peak in the morning, independent of  $\text{NO}_x$  and  $\text{NO}_y$ , while all three species peak together in the evening at about 7:00 p.m.

While  $\text{NH}_{x,\text{gas}}$  usually reaches its maximum concentration before  $\text{NO}_x$  and  $\text{NO}_y$ , and  $\text{NO}_x$  and  $\text{NO}_y$  usually have only a single maximum during the day, Figure 6d shows an example of  $\text{NO}_x$  and  $\text{NO}_y$  having a morning peak at about 9:00 a.m., followed by an afternoon peak at about 3:00 p.m.  $\text{NH}_{x,\text{gas}}$  shows very little variability in the morning but similar variability to  $\text{NO}_x$  and  $\text{NO}_y$  in the afternoon.

Figure 6e should be compared to Figure 6f. In both cases,  $\text{NO}_x$  and  $\text{NO}_y$  increase throughout the day, starting at 7:00 a.m., with the difference being that  $\text{NO}_x$  and  $\text{NO}_y$  have similar concentrations on JD = 153, while on JD = 120  $\text{NO}_x$  and  $\text{NO}_y$  concentrations are the same during the morning hours but diverge significantly starting at 11:00 a.m. This divergence continues throughout the day until  $\text{NO}_y$  concentrations are nearly twice those of  $\text{NO}_x$ . This of course implies the presence of oxidized nitrogen species other than  $\text{NO}$  and  $\text{NO}_2$  at significant levels. On JD = 153,  $\text{NH}_{x,\text{gas}}$  decreases throughout the day, while on JD = 120,  $\text{NH}_{x,\text{gas}}$  concentrations peak around noon.

Finally, Figure 6g, a plot of  $\text{NH}_{x,\text{gas}}$ ,  $\text{NO}_x$ , and  $\text{PM}_1$  ( $\mu\text{g}/\text{m}^3$ ), shows that  $\text{PM}_1$  also has similar diurnal patterns as gas species. The diurnal cycling of all aerosol species suggests daily cycling of the boundary layer bringing aerosols generated along the Front Range into the park.

### Comparison of $\text{NH}_{x,\text{gas}}$ chemiluminescence to $\text{NH}_3$ URG measurements

In Table 2, 24-hr average  $\text{NH}_{x,\text{gas}}$  as measured by chemiluminescence is about a factor of 4–5 greater than 24-hr  $\text{NH}_3$  derived from the URG denuder method.  $\text{NH}_{x,\text{gas}}$  is derived by differencing a chemiluminescence measurement of total nitrogen ( $\text{TN}_x$ , reduced + oxidized), after passing through a Nylasorb filter, and a modified  $\text{NO}_y$  measurement. The Nylasorb filter removes particles such as  $\text{NH}_4\text{NO}_3$  as well as  $\text{HNO}_3$  gas. The  $\text{NO}_y$  instrument does not have a filter in the air stream, so it is responsive to  $\text{NH}_4\text{NO}_3$  as well as  $\text{HNO}_3$ . Therefore, to derive an estimate of  $\text{NH}_{x,\text{gas}}$  that includes  $\text{HNO}_3$  and particle  $\text{NO}_3$ , these two species are added to the difference of the measured  $\text{TN}_x$  and  $\text{NO}_y$ . It is these values that are reported in Table 2.

The straightforward interpretation of  $\text{NH}_{x,\text{gas}}$  significantly exceeding  $\text{NH}_3$  is that there are significant concentrations of reduced nitrogen gas species other than  $\text{NH}_3$ . However, there

are at least two artifacts associated with the  $\text{NH}_{x,\text{gas}}$  estimate that could lead to an inflated measured concentration. First, the  $\text{NO}_y$  measurement was made with the molybdenum-catalyzed converter set to 285°C instead of the recommended 315°C, so all oxidized nitrogen may not have been converted, and hence the  $\text{NO}_y$  is a lower bound estimate of total oxidized nitrogen. Therefore  $\text{TN}_x - \text{NO}_y$  could contain oxidized nitrogen species and be an overestimate of  $\text{NH}_{x,\text{gas}}$ . Second, the  $\text{NH}_{x,\text{gas}}$  measurement was made using an airstream with an inline Nylasorb filter. Ammonium nitrate particles collected during lower nighttime temperatures are undoubtedly volatilized during higher daytime temperatures, causing a positive artifact in the  $\text{NH}_{x,\text{gas}}$  measurement. It can be seen in Table 2 that the backup filter used to measure volatilized ammonium from ammonium nitrate collected on the primary filter in the URG system shows that the concentrations of volatilized ammonium were nearly as high as the ammonium on the primary front filter. These backup filter ammonium concentrations should be indicative of the amount of ammonium volatilized from the inline filter used for the  $\text{NH}_{x,\text{gas}}$  measurement, depending, of course, on the relative temperature difference between the filter holders for the Nylasorb substrate of the  $\text{NH}_{x,\text{gas}}$  and the URG system.

If it is assumed that measured  $\text{NH}_{x,\text{gas}}$  is an overestimation and that  $\text{NH}_{x,\text{gas}}$  for the most part is primarily  $\text{NH}_3$ , the  $\text{NH}_{x,\text{gas}}$  measurements are normalized to the URG measured  $\text{NH}_3$  using

$$\text{NH}_{3,\text{urg}} = a_1 \text{NH}_{x,\text{gas}} - \text{NH}_{3,\text{urgback}} \quad (1)$$

An OLS linear regression solution to eq 1 yields  $a_1 = 0.25 \pm 0.006$  and  $R^2 = 0.45$ . Figure 7 shows a temporal plot of the normalized  $\text{NH}_{x,\text{gas}}$  and  $\text{NH}_{3,\text{urg}}$  measurements. For the most part, the agreement between the two measurements is good. There are two or three multiday episodes during the summer when  $\text{NH}_{x,\text{gas}}$  measurements show elevated concentrations and the  $\text{NH}_3$  measurements do not. These are possible cases in which there may be elevated levels of reduced nitrogen other than  $\text{NH}_3$  gas.

### Approach to Apportioning Ammonia to its Emission Sources

The approach taken in this analysis to apportion measured concentrations of various aerosol species at a receptor site to emission sources is to combine modeled transport and dispersion of a conservative tracer released in proportion to emissions with receptor-oriented models to statistically account for removal and chemical processes. From these relationships, the average contributions of source regions throughout North America to the receptor concentration over a period of time are assessed. The goal of the analysis is to separate the contributions from nearby local sources, sources along the Front Range, and other source regions east and west of the Continental Divide.

The tracer modeling system consists of three major components: WRF (Weather Research and Forecasting Model) (Skamarock et al., 2008), a regional weather model; CAMx (Comprehensive Air Quality Model with Extensions) (Environ, 2011), a chemical transport model; and a detailed emission inventory (Adelman and Omary, 2011). WRF (Skamarock

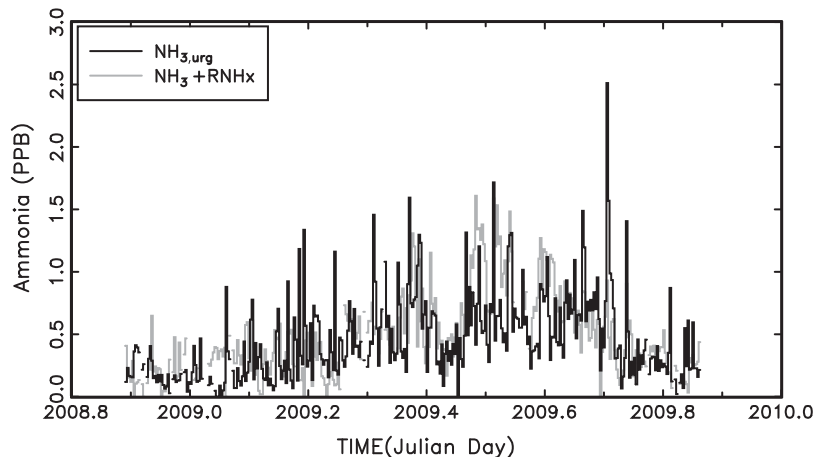


Figure 7. Temporal plot of  $\text{NH}_3$  derived from the URG sampler and the chemiluminescence measurement of  $\text{NH}_{x,\text{gas}}$  normalized to the URG  $\text{NH}_3$  data.

et al., 2008) was used to generate hourly meteorological fields on three nested domains of 34 vertical layers and horizontal grid sizes of 36, 12, and 4 km. WRF was initialized with the North American Regional Reanalysis (NARR) data (Mesinger et al., 2006; NARR, 2009). NARR data were also used for analysis nudging on the coarse domain. Data for observational nudging on the 4-km domain were from the Meteorological Assimilation Data Ingest System (MADIS) data set, as well as meteorological data collected as part of RoMANS, including data from a 10-m tower at the core site and a radar wind profiler in Estes Park, CO. Major physics options used in WRF were the rapid radiative transfer model (RRTMG) microphysics (Mlawer et al., 1997), the Kain–Fritsch cumulus parameterization (Kain and Fritsch, 1993; Kain, 2004) on the two coarse domains, the five-layer thermal diffusion land surface model (Dudhia, 1996), and the Yonsei University planetary boundary layer scheme (Hong et al., 2006; Hong and Kim, 2008).

Tracer emissions are based on the ammonia emission inventory developed by the Western Regional Air Partnership (WRAP), the National Emission Inventory (NEI), and are updated to reflect the nested RoMANS model domains and time period (Adelman and Omary, 2011). The major sources within the ammonia emission inventory are livestock operations, agricultural fertilizer applications, and mobile sources.

The tracer simulation was conducted using the WRF and ammonia emissions as inputs to CAMx. CAMx is an Eulerian grid air quality model that is often used to investigate regional air pollution. CAMx was modified to simulate an arbitrary number of conserved tracers, with no loss through chemical transformation or deposition. As shown in Figure 8, the inert  $\text{NH}_3$  tracer transport simulation was conducted for 107 different source regions throughout North America. The source regions were selected by centering them on high  $\text{NH}_3$  emission regions, based on the 2002 WRAP annual average  $\text{NH}_3$  emissions

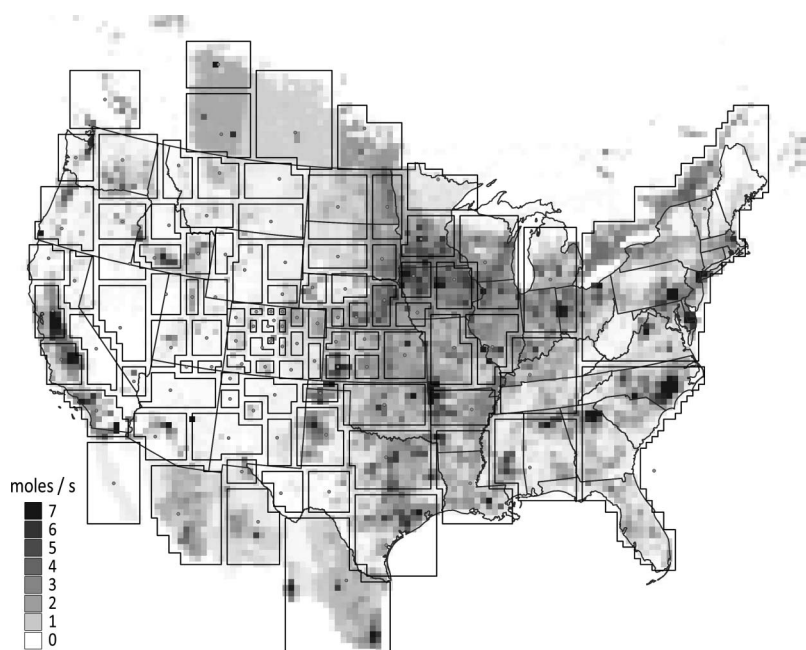


Figure 8. Source regions and ammonia emission inventory used in the conservative “tracer” analysis.

inventory. Many areas with little or no NH<sub>3</sub> emissions were excluded. The smallest source regions are near RMNP, and they generally increased in size with distance from the park. Ten source regions were selected within Colorado, including one at RMNP, the neighboring population center at Estes Park, CO, and Denver, CO, as well the agricultural regions in north-eastern Colorado.

## The receptor model

The starting point for the attribution analysis is the concentrations,  $C_{ki}$ , of modeled ammonia tracer for 1-hr time periods,  $k$ , for 107 source areas,  $i$ . The bases of most apportionment models rely on the assumption that the concentration of airborne aerosol species can be described by the sum of a number (hopefully, small) of source area vectors. The equation for this description is

$$C_{ki} = \sum_j a_{kj} S_{ji} + \varepsilon_{ik} \quad (2)$$

where  $k = 1 \dots m$ , the number of observations;  $i = 1 \dots n$ , the number of source area patterns contributing to the receptor;  $j = 1 \dots N$ , the number of source areas;  $C_{ki}$  = concentrations of ammonia from source area patterns  $i$  for time period  $k$ ;  $a_{kj}$  = time-weighting functions;  $S_{ji}$  = source vectors; and  $\varepsilon_{ik}$  = error term including random and lack of fit error.

The source vectors are essentially weighting factors that group source areas together into larger source regions or transport pathways that on the average contribute to elevated concentrations of trace species under certain various, unique types of meteorological conditions.

When source vectors are unknown, it is sometimes possible to gain insight into source–receptor relationships through the use of a singular value decomposition of  $C_{ki}$  (Golub and Reinsch, 1970):

$$C_{ki} = \sum_{j=1}^m u_{kj} S_j \nu_{ji} + \sum_{j=m}^n u_{kj} S_j \nu_{ji} \quad (3)$$

Comparison of eqs 2 and 3 suggests

$$S_{ji} = \nu_{ji} \quad (4)$$

$$a_{kj} = u_{kj} S_j \quad (5)$$

and

$$\varepsilon_{ik} = \sum_{j=m}^n u_{kj} S_j \nu_{ji} \quad (6)$$

where  $s_j$  = the singular values and  $u_{kj}$ ,  $\nu_{ji}$  = the eigenvectors,  $m$  = the number of unique eigenvectors, and  $\varepsilon_{ik}$  = the error term described earlier.

Therefore, the eigenvectors,  $\nu_{ji}$ , are the source vectors as derived from the modeled concentrations of ammonia at the receptor site over time. The source vectors,  $S_{ji}$ , are basic patterns found in the modeled data set and are reflective of transport patterns resulting from reoccurring meteorological patterns.

Similar eigenvector analyses have been used where  $C_{ki}$  are measured concentrations of a species of interest, measured at a number of monitoring sites over time to estimate the relative contribution of source regions to measured aerosol levels at the measurement sites. However, in this case, the  $C_{ki}$  are modeled inert concentrations. There are a variety of ways the preceding analysis can be used to approximately apportion the species of interest, in this case ammonia, to the various source regions.

In the following analysis, the eigenvectors are used to group various source regions into larger regions that represent transport from that larger region. These identified groups of source regions are then averaged together for each time period (typically, 1 hr) and treated as independent variables in a regression model where the dependent variables are the measured concentrations of the aerosol of interest and the averaged source regions are the independent variables:

$$(NH_3)_k = \sum_j \alpha_{jk} \Phi_{jk} \quad (7)$$

where  $NH_3$  = the measured hourly or average 24-hr ammonia concentrations,  $\alpha_{jk}$  = the regression coefficients, and  $\Phi_{jk}$  = the average of modeled concentrations arriving at the receptor from source areas, grouped according to eigenvectors,  $\nu$ .

## A first-order apportionment estimate to easterly and westerly transport

Wind and pollution roses using measured hourly surface wind directions at RMNP can be used to examine the wind direction frequency over the year and the average ammonia concentrations associated with each wind direction (Figure 9). Comparison of the continuous NH<sub>3</sub> to URG values showed a systematic offset of ~0.6 PPB. Consequently, the continuous data were reduced by this amount. As shown in Figure 9a, the winds were predominantly from a northwestern or southeastern direction. These surface winds are channeled by the local terrain turning the surface winds by ~60 degrees. If easterly winds are defined as being between 60 to 240 degrees, only 28% of the winds were from the east. However, easterly winds were associated with higher NH<sub>3</sub> concentrations, with an annual average NH<sub>3</sub> of 3 PPB, compared to 1.9 PPB for westerly winds.

The product of the wind and pollution roses is the contribution of the ammonia for a given wind sector to the average NH<sub>3</sub> and is plotted in Figure 9b as the relative contribution. This gives a semiquantitative estimate of the contributions from sources in a given wind sector. Integration over easterly winds (60–240 degrees) and westerly winds (240–60 degrees) suggests that 44% and 56% of the NH<sub>3</sub> came from sources east and west of RMNP, respectively. The lowest easterly contribution is in the winter at 29% and highest in the fall at 49%. These results are summarized in Table 3. These percentages are likely an upper bound on the contributions from sources east of RMNP. The

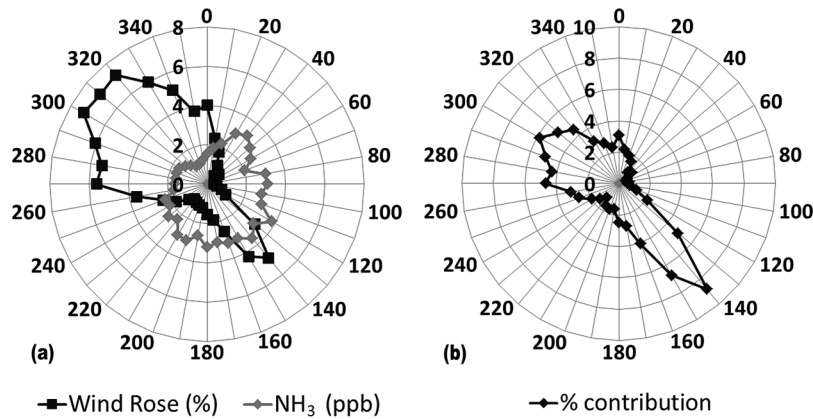


**Figure 9.** (a) Frequency at which the measured surface winds at RMNP are from a given direction and the average  $\text{NH}_3$  concentrations associated with each wind direction. (b) Average contributions of the  $\text{NH}_3$  concentrations associated with each wind sector to the RMNP annual average  $\text{NH}_3$ .

**Table 3.** The estimates of the contribution of sources east and west of RMNP to the seasonal and annual measured  $\text{NH}_3$  concentrations

| Sources | Winter | Spring | Summer | Fall | Annual |
|---------|--------|--------|--------|------|--------|
| East    | 29%    | 44%    | 45%    | 49%  | 44%    |
| West    | 71%    | 56%    | 55%    | 51%  | 56%    |

frequency of easterly winds includes low wind speeds that would contain large local source contributions. In addition, transport from the east often includes trajectories that originate west of RMNP, and therefore, some fraction of the  $\text{NH}_3$  concentrations associated with the easterly surface winds will be from sources west of RMNP. This bias is offset by the fact that westerly winds will have contributions from sources east of RMNP. However, this is expected to be relatively small due to the lower frequency of transport from the east.

### CAMx modeled concentrations

The CAMx model was run as described in the previous section with the 107 source regions shown in Figure 8 and without deposition and chemistry. A first-order calculation of

ammonia lost to deposition was estimated using  $C \cdot \exp(-kt)$ , where  $C$  is the modeled inert tracer concentration without deposition,  $k = v_d/H$ , where  $v_d$  is the deposition velocity and  $H$  is the scale height, and  $t$  is transport time. Transport time was estimated assuming an average transport velocity of 5 m/sec and an average deposition velocity of 1.0 cm/sec.

Although modeled ammonia concentrations show some diurnal variability on most days and pronounced variability on other days, they do not systematically predict observed diurnal variability of almost all aerosol species on nearly every day that measurements were made. Therefore, in the analysis that follows, 24-hr average concentrations of both modeled and measured concentrations will be used.

Figure 10 is a temporal plot of 24-hr average URG measured and modeled ammonia with estimated deposition, and Table 4 shows the summary statistics for modeled and measured ammonia. Notice that, on the average, modeled and measured ammonia agree surprisingly well in that modeled ammonia is about 50% less than measured. The agreement may be fortuitous, given all the assumptions concerning emission rates, simplifying assumptions concerning deposition, and not having chemistry in the model.

In general, the temporal agreement is also surprisingly good, with an overall correlation between measured and modeled

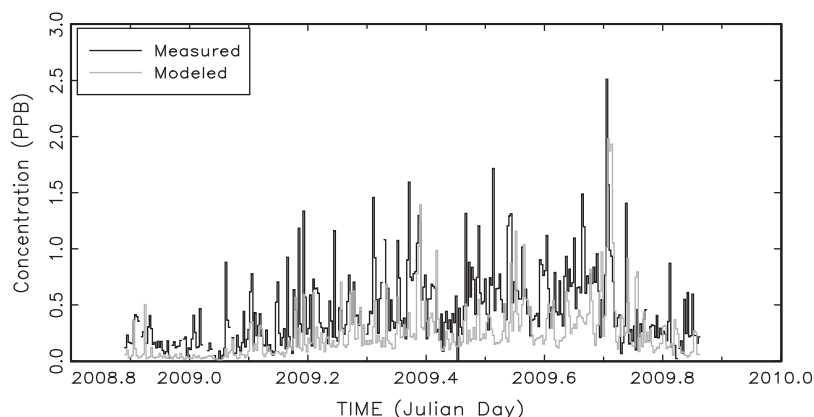


**Figure 10.** Time series of measured  $\text{NH}_3$  and  $\text{NH}_3$  estimated from the CAMx tracer data.

**Table 4.** Statistical summary of URG NH<sub>3</sub> and NH<sub>3</sub> estimated from the CAMx tracer data

| Variable                      | Std  |      | Minimum | Maximum | Valid |
|-------------------------------|------|------|---------|---------|-------|
|                               | Mean | dev  |         |         |       |
| NH <sub>3</sub> (ppb)         | 0.45 | 0.34 | 0.12    | 2.51    | 340   |
| Modeled NH <sub>3</sub> (ppb) | 0.25 | 0.27 | 0.07    | 1.98    | 340   |

**Table 5.** Fractional contribution from various source regions as predicted by the model with simple first-order deposition estimates and by the receptor model

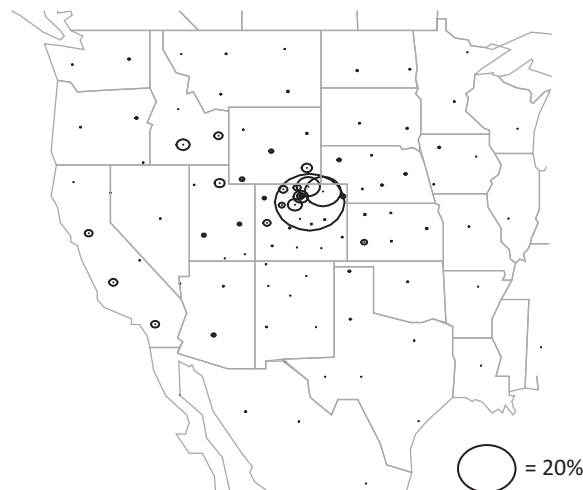
| Region           | Modeled | Receptor |
|------------------|---------|----------|
| All CO           | 0.53    | 0.51     |
| Outside CO       | 0.47    | 0.49     |
| Front Range CO   | 0.27    | 0.15     |
| Northeast CO     | 0.12    | 0.04     |
| Southeast CO     | 0.01    | 0.01     |
| West CO          | 0.05    | 0.11     |
| Central CO       | 0.04    | 0.14     |
| Yampa            | 0.04    | 0.05     |
| Midwest          | 0.02    | 0.01     |
| Texas            | 0.01    | 0.01     |
| New Mexico       | 0.01    | 0.02     |
| Arizona          | 0.01    | 0.04     |
| California       | 0.07    | 0.12     |
| Snake River      | 0.06    | 0.07     |
| Washington state | 0.02    | 0.02     |
| Canada           | 0.01    | 0.01     |
| Nebraska         | 0.03    | 0.01     |
| Kansas           | 0.04    | 0.00     |
| Utah             | 0.07    | 0.10     |
| Wyoming          | 0.05    | 0.03     |
| Montana          | 0.02    | 0.01     |
| Mexico           | 0.01    | 0.02     |

ammonia of 0.37. If the data are averaged to a week, the correlation between measured and modeled is 0.75. For the most part, weekly and seasonal variability is captured by the model.

Table 5 and Figure 11 show modeled relative apportionment of ammonia. “Front Range” refers to the northern front range of the Colorado Rockies, and “northeastern Colorado” refers to regions 184 and 197 in Figure 8. The Front Range and northeastern Colorado include the large confined animal feeding operations (CAFO) around Greeley, Kersey, Fort Morgan, and Brush, Colorado. This region of the United States is predicted to contribute 35% of all measured ammonia at RMNP. Other CAFOs in western Colorado and the Yampa River valley of Colorado also contribute significantly, as does the Snake River basin in southern Idaho, eastern Utah, and as far away as California.

### Receptor Model Apportionment of Ammonia

As stated already, the goal of the eigenvector analysis is to identify those groups of source regions that transport to the

**Figure 11.** Relative average contributions of various source regions to modeled ammonia at the receptor site. The location of each circle corresponds to the centroid of a source area, while the size of the circle represents the fractional contribution of the source area to the average ammonia concentration at RMNP. The largest circle corresponds to the northern Front Range of Colorado and represents a 27% contribution.

receptor site during some given time period. The modeled inert tracer concentrations for each source region are normalized to the mean concentration for that site:

$$Z_{kj} = C_{kj} / \bar{C}_j \quad (8)$$

where as before,  $k$  = a time index, while  $j$  refers to a site.

A singular value decomposition calculation is carried out on the  $Z_{kj}$  matrix. Because the eigenvectors vary to some degree based on the time increment chosen for the eigenvector extraction, the data were broken down on a seasonal basis. Because the first 10 eigenvectors typically explained more than 80% of the variance, they were used in the analysis. After weighting the modeled concentrations for deposition, the sources in each region represented by the eigenvectors were averaged together to form the independent variables in the regression model represented by eq 7.

Four typical spatial eigenvectors are shown in Figure 12. The relative sizes of the circles are proportional to the eigenvector weightings, and the center of each circle corresponds to the centroid of the source regions shown in Figure 8. These eigenvectors correspond to typical average transport pathways for the 24-hr averaging time period of the modeled tracer concentrations. Figure 12a corresponds to a general transport pattern from the southwest that includes source areas in western Colorado, Nevada, Arizona, and Mexico. Figure 12b shows more of a stagnant upslope condition with some transport from the Midwest, while 12d also corresponds to an upslope condition but with prior transport from western Colorado, southeastern Wyoming, and western Nebraska. Figure 12c shows transport from the Snake River valley of southern Idaho as well as some transport from the southwest.

Because the chemiluminescence estimation of NH<sub>x,gas</sub> may contain other reduced species of N than NH<sub>3</sub>, both NH<sub>x,gas</sub>, as represented by the chemiluminescence measurement, and NH<sub>3</sub>,

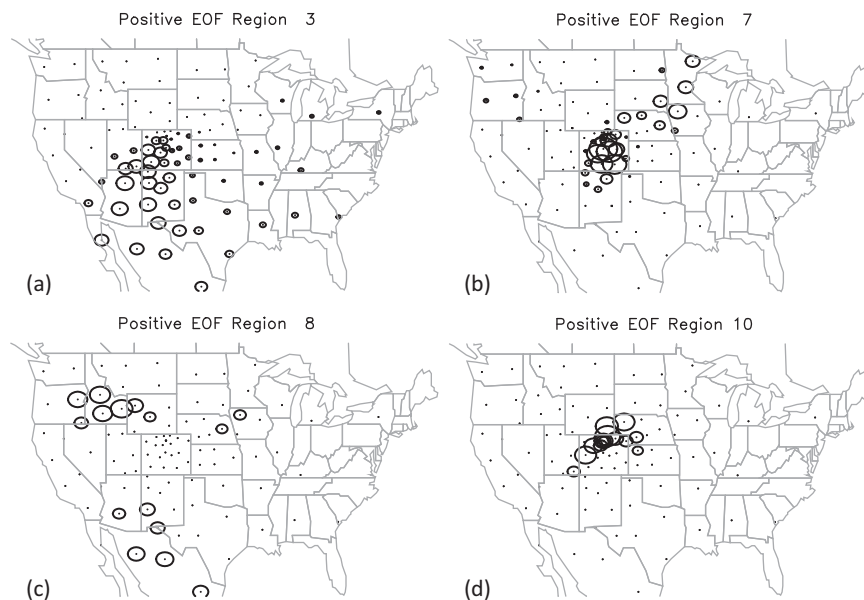


**Figure 12.** Four eigenvectors corresponding to typical transport pathways. Each circle corresponds to a source area, while the size of the circle corresponds to the relative weight of that source area to the eigenvector represented. Transport of emissions from those source areas with the same size circles is correlated in time and therefore is averaged together to represent one large source region.

**Table 6.** Summary statistics for an OLS regression between receptor modeled and measured ammonia concentrations

|      |        | $R^2$ | Slope | Std error | $t$ -Value |
|------|--------|-------|-------|-----------|------------|
| URG  | Winter | 0.49  | 1.00  | 0.06      | 17.55      |
| CHEM | Spring | 0.58  | 1.00  | 0.04      | 27.24      |
| URG  | Summer | 0.21  | 1.00  | 0.05      | 19.97      |
| CHEM | Fall   | 0.74  | 1.00  | 0.05      | 19.78      |

derived from the URG instrument, were used in the regression. However, because the chemiluminescence measurement was normalized to the URG  $\text{NH}_3$  data, the relative amount of reduced N species other than  $\text{NH}_3$  cannot be inferred. For those cases in which there is a better correlation between  $\text{NH}_{x,\text{gas}}$  and modeled tracer concentrations than between  $\text{NH}_3$  and tracer data, only the possibility of reduced gaseous N species other than  $\text{NH}_3$  can be inferred.

The apportionment results corresponding to the model with the highest coefficient of determination,  $R^2$ , are reported. The results of these regressions are summarized in Table 6, in which a statistical summary of the regression model comparing measured to predicted  $\text{NH}_{x,\text{gas}}$  concentrations is presented for each season. The first column indicates whether the URG or chemiluminescence data yielded the highest  $R^2$ . For the spring and fall months, the correlation between chemiluminescence-measured  $\text{NH}_{x,\text{gas}}$  and tracer data is higher than for URG  $\text{NH}_3$ , suggesting the presence of some reduced species other than  $\text{NH}_3$ , or perhaps the chemiluminescence measurement has more precision than the URG measurement. In any case, although not explicitly presented here, the apportionment to source regions is similar for either the URG or chemiluminescence measurement.

Figure 13 shows the time series of model predictions and URG  $\text{NH}_3$  or normalized  $\text{NH}_{x,\text{gas}}$  chemiluminescence data. Concentrations are in PPB. The spring time period, Figure 13b, corresponded to the season with the second highest average concentration, with one 9-day episode exceeding or near the 1.0 PPB concentration level. During this time period, tracer model results compared more favorably with the chemiluminescence measurement because of two factors. First, there are a number of single-day excursions that show up in the URG data but not the chemiluminescence measurements. These excursions are not predicted by the receptor model. Second, during the last quarter of the season, the chemiluminescence measurement showed four days of elevated  $\text{NH}_{x,\text{gas}}$  significantly above  $\text{NH}_3$  levels that were also predicted by the receptor model. This is suggestive of reduced gaseous N species other than  $\text{NH}_3$ .

Figure 13c shows the concentration timelines for the summer season. The correspondence between receptor model and measured concentrations is lowest during the summer time period, possibly because of daily mixing of Front Range emissions up to the receptor site that is not fully captured by the WRF wind-fields. As discussed previously, modeled wind fields are able to capture some vertical mixing associated with diurnal transport but not all. Figure 13d is the concentration timeline for the fall season. It is made up of two episodes in early fall that correspond to transport from the northwest across the Rocky Mountains, northeastern Colorado, and on into the receptor site. The correlation between measurements and the receptor model is highest during this season at over 0.86.

The apportionment estimates are summarized in Table 7 and Figures 14 and 15. Table 7 shows the apportionment of  $\text{NH}_{x,\text{gas}}$  (primarily  $\text{NH}_3$ ) in PPT to the various source regions for each season of the year, as well as an overall yearly apportionment. The last column is the fraction of  $\text{NH}_{x,\text{gas}}$  apportioned to each

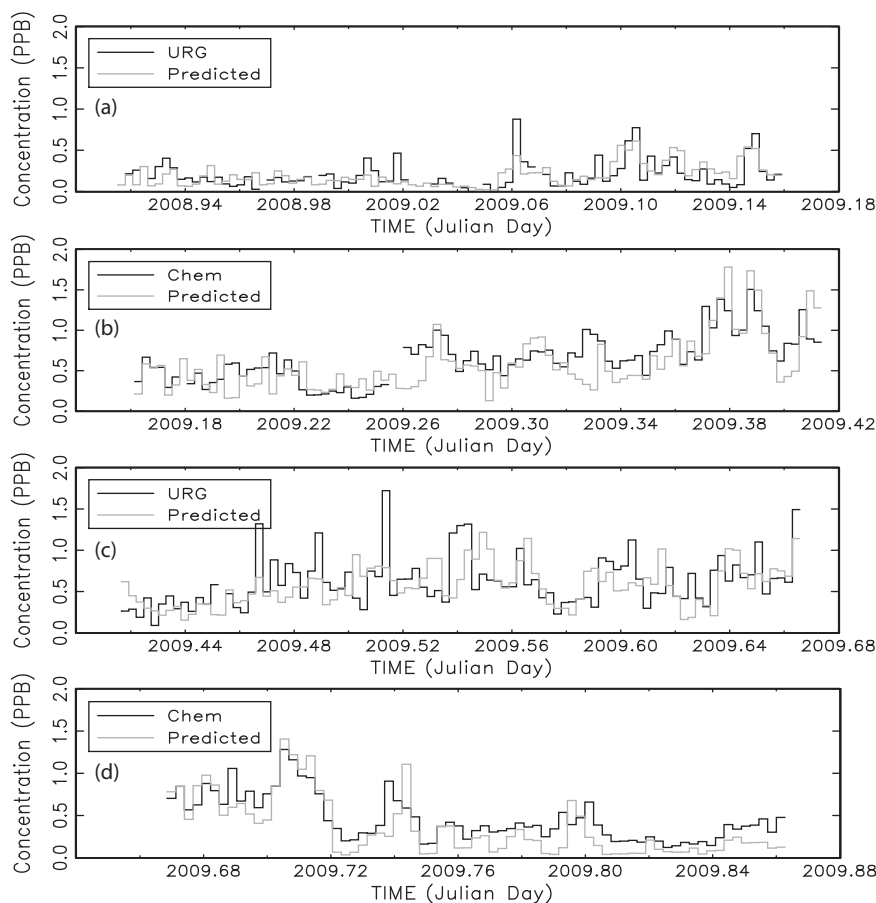


**Figure 13.** Temporal plot of 24-hr average URG  $\text{NH}_3$ , normalized chemiluminescence (Chem)-derived  $\text{NH}_{x,\text{gas}}$ , and receptor-modeled normalized  $\text{NH}_{x,\text{gas}}$  or  $\text{NH}_3$ , depending on whether the URG or chemiluminescence data were used as the dependent variable in the OLS regression. Each panel represents a season, and the order of the panels is winter, spring, summer, and fall.

region. The first two rows show the relative apportionment to sources inside and outside Colorado, and the same data are summarized in Figure 14. Overall, there is approximately a 50–50 split of ammonia arriving at the receptor site from inside versus outside Colorado. During the winter, spring, and fall seasons, more ammonia is associated with sources inside Colorado, significantly so during the winter time period. During the summer season, transport from outside Colorado's borders becomes more significant. Averaging across the seasonal averages yields apportionments of about 54% versus 46% from inside and outside of Colorado, respectively. If the inside and outside apportionments are weighted to concentrations, the split is about 51% versus 49%, respectively.

The transport of ammonia to the receptor site is primarily influenced by westerly transport. Although some of the largest emissions of ammonia are found in the Midwest and the eastern part of the United States, these sources apparently contribute little to measured ammonia at the receptor site, while sources to the west are major contributors. This trend is true for all seasons. The source areas outside the borders of Colorado that contribute most to ammonia concentrations are California and northeastern Utah, where there are large CAFO activities. CAFO operations along the Snake River valley in southern Idaho are the next largest out-of-state contributor to ammonia.

Within the state of Colorado, the hybrid receptor modeling results suggest that the Front Range and western and central Colorado all contribute about equally during the spring and summer months, while during the winter season, western and central Colorado contribute more, relative to the Front Range. The Snake River valley is also one of the largest contributors during the spring season. During the fall season, the Front Range and California are the largest contributors, with northeastern, western, and central Colorado contributing slightly less ammonia. Synoptic-scale upslope conditions transported significant amounts of ammonia into the receptor site from CAFO operations along the northern Front Range and northeastern Colorado. These transport conditions were associated with wind trajectories that extended over northeastern Colorado and back across the northwestern United States. Consequently, during these time periods, the Snake River valley, California, and Utah also contributed significantly. During the summer, California contributes significantly, with the Front Range, Utah, and western and central Colorado contributing somewhat less but still quite significantly. The winter season has the western sources contributing most of the measured ammonia.

On the average, northeastern Colorado, including the Front Range, is predicted to contribute about 19% of measured ammonia, with western and central Colorado each contributing 11%

**Table 7.** Amount of ammonia in PPT apportioned to various source regions as a function of season as well as the average fraction of ammonia apportioned to each source region; also shown is the apportionment to all sources in the state of Colorado

| Region                      | Spring | Summer | Fall   | Winter | Average | Fraction |
|-----------------------------|--------|--------|--------|--------|---------|----------|
| All CO (ppt)                | 297.14 | 364.11 | 198.87 | 127.65 | 246.94  | 0.51     |
| Outside CO (ppt)            | 285.49 | 463.41 | 150.03 | 68.73  | 241.91  | 0.49     |
| Front Range CO (ppt)        | 81.57  | 132.40 | 69.78  | 11.78  | 73.88   | 0.15     |
| Northeast CO (ppt)          | 34.96  | 8.28   | 38.38  | 1.96   | 20.89   | 0.04     |
| Southeast CO (ppt)          | 5.83   | 8.28   | 0.00   | 0.00   | 3.53    | 0.01     |
| West CO (ppt)               | 40.78  | 82.75  | 45.36  | 53.02  | 55.48   | 0.11     |
| Central CO (ppt)            | 104.87 | 91.03  | 38.38  | 39.28  | 68.39   | 0.14     |
| Yampa (ppt)                 | 23.30  | 49.65  | 3.49   | 17.67  | 23.53   | 0.05     |
| Midwest (ppt)               | 5.83   | 8.28   | 0.00   | 0.00   | 3.53    | 0.01     |
| Texas (ppt)                 | 0.00   | 8.28   | 3.49   | 0.00   | 2.94    | 0.01     |
| New Mexico (ppt)            | 11.65  | 16.55  | 10.47  | 9.82   | 12.12   | 0.02     |
| Arizona (ppt)               | 17.48  | 24.83  | 17.45  | 15.71  | 18.86   | 0.04     |
| California (ppt)            | 17.48  | 165.50 | 52.34  | 7.86   | 60.79   | 0.12     |
| Nevada (LV) (ppt)           | 0.00   | 8.28   | 3.49   | 0.00   | 2.94    | 0.01     |
| Snake River (ppt)           | 87.39  | 41.38  | 10.47  | 0.00   | 34.81   | 0.07     |
| Washington state (ppt)      | 34.96  | 8.28   | 3.49   | 0.00   | 11.68   | 0.02     |
| Canada (ppt)                | 5.83   | 0.00   | 3.49   | 1.96   | 2.82    | 0.01     |
| Nebraska (ppt)              | 0.00   | 8.28   | 3.49   | 0.00   | 2.94    | 0.01     |
| Kansas (ppt)                | 5.83   | 0.00   | 0.00   | 3.93   | 2.44    | 0.00     |
| Oklahoma and Arkansas (ppt) | 0.00   | 0.00   | 0.00   | 0.00   | 0.00    | 0.00     |
| Utah (ppt)                  | 64.09  | 82.75  | 20.93  | 25.53  | 48.33   | 0.10     |
| Wyoming (ppt)               | 5.83   | 49.65  | 10.47  | 0.00   | 16.49   | 0.03     |
| Montana (ppt)               | 11.65  | 8.28   | 3.49   | 0.00   | 5.85    | 0.01     |
| Mexico (ppt)                | 5.83   | 24.83  | 6.98   | 3.93   | 10.39   | 0.02     |

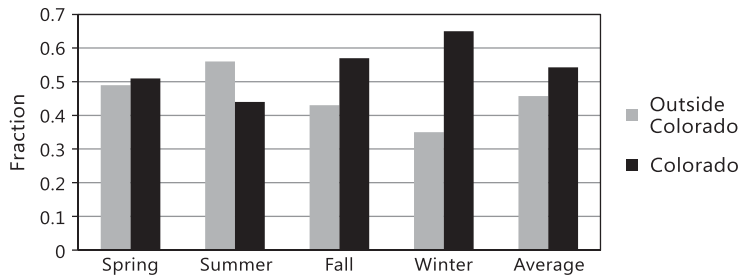


**Figure 14.** Fraction of ammonia apportioned to the receptor site from sources in and outside of Colorado as predicted by the hybrid receptor model.

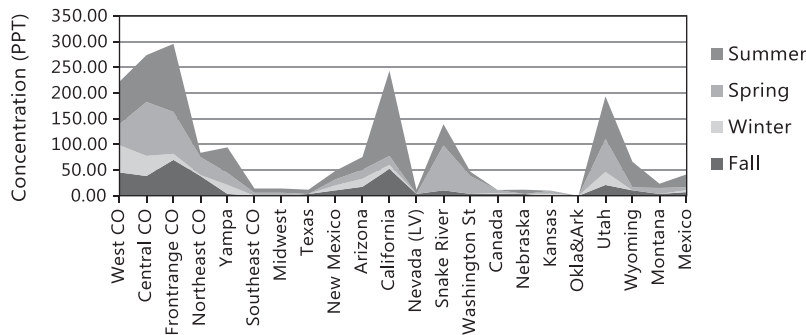


**Figure 15.** Receptor modeling apportionments of contributions of various source regions to the receptor site as a function of season.

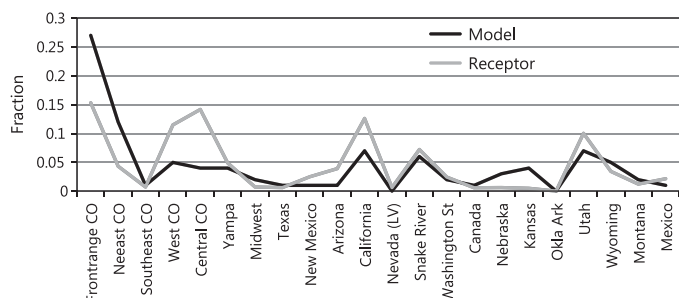


**Figure 16.** Receptor modeling apportionment results compared to the apportionment predictions of the tracer CAMx modeled concentrations that have been weighted for dry deposition.

and 14%, respectively. The Yampa River valley contributes another 5%.

It is informative to compare the receptor modeling results to the tracer CAMx concentrations weighted for deposition. These comparisons are shown in Figure 16. There is an overall general agreement between tracer data weighted for deposition and results of the hybrid receptor model. However, the tracer model suggests about a 39% contribution from the northern Front Range and northeastern Colorado, while the receptor model estimate is below 20%. The receptor model apportions more ammonia to western and central Colorado than does the tracer receptor model. This trend is also true for California and Arizona sources, with the tracer receptor model apportioning about twice as much to these states as the CAMx tracer model.

The systematic correlation between diurnally varying local easterly winds measured at the receptor site and diurnal increases in measured  $\text{NH}_{x,\text{gas}}$  concentrations suggests Front Range transport into the receptor area due to systematic daily mixing of Front Range air into the receptor area. Back-trajectory analysis shows that most transport to the receptor site is a result of transport from the various source areas in the West to the Front Range and then back into the receptor area, carrying both emissions from more distant sources as well as Front Range emissions. Therefore, it is the combination of more distant and local sources along the Front Range ultimately mixing in the receptor area that determines the relative contributions of these sources to nitrogen at the receptor site. Modeled wind fields have to capture not only the westerly transport to the Front Range but also the mixing of these air masses into the park.

The eigenvectors show independent strong correlations between source areas to the west and sources to the northeast but do not capture the systematic daily transport of both pathways into the park. As such, Front Range source regions do not correlate well with individual western source regions and therefore do not fall into transport pathways from the west but into a separate eigenvector. When averaging the source regions represented by the various eigenvectors, Front Range source regions are averaged together. This time series of concentrations is not as well correlated as transport from source regions near and west of the receptor site and therefore do not result in a statistically

significant relationship with measured concentration data. Consequently, the receptor modeling results may be an underestimate of the Front Range contribution to  $\text{NH}_{x,\text{gas}}$  concentrations at the receptor site.

## Summary

In Rocky Mountain National Park (RMNP), both wet nitrate deposition and ammonium deposition have increased over the last 20 years. The Rocky Mountain Atmospheric Nitrogen and Sulfur (RoMANS) study was initiated to better understand the origins and physical/chemical characteristics of nitrogen species, as well as the complex chemistry occurring during transport from source to receptor. Increases in ammonia emissions tend to increase and change the composition of particulate matter (PM) mass concentrations. Regardless of the chemical form and phase of the nitrogen, it will ultimately be deposited onto terrestrial or aquatic surfaces. However, where these species are deposited does depend on the chemical form and phase of the nitrogen. For example, gaseous ammonia has higher deposition rates and will deposit closer to the sources, while ammoniated particulates can be transported hundreds of kilometers before deposition.

As part of the study, a monitoring program was initiated for one year starting in November 2008. The monitoring program consisted of intensive, high time resolution measurements of particles, gas, wet deposition, and meteorology at a core site in RMNP.

Gas-phase measurements were made continuously and in real time, with 1-min averaged data. Instruments were collocated with the existing IMPROVE and CASTNET sites near the eastern boundary of RMNP. Continuous measurements included an estimation of nitric acid ( $\text{HNO}_3$ ), reduced nitrogen gaseous species including ammonia ( $\text{NH}_{x,\text{gas}}$ ), nitrogen oxides ( $\text{NO}_x$ ),  $\text{NO}_y$  compounds ( $\text{NO}_x$  plus other reactive oxidized nitrogen species), and carbon monoxide (CO). Calibrations for most instruments were performed on an almost daily basis. For  $\text{NH}_{x,\text{gas}}$ , a calibration was done before, once during, and after the study.

The approach taken in this analysis to apportion emission sources to measured concentrations of various aerosol species at a receptor site combines modeled transport and dispersion of a conservative tracer released in proportion to ammonia emissions, with receptor-oriented models to statistically account for removal and chemical processes. From these relationships the average contributions of source regions throughout North America to the receptor concentration over a period of time were assessed. The goal of the analysis is to separate out the contributions from nearby local sources, sources along the Front Range, and other source regions east and west of the Continental Divide.

The tracer modeling system consists of three major components: WRF (Weather Research and Forecasting Model; Skamarock et al., 2008), a regional weather model; CAMx (Comprehensive Air Quality Model with Extensions; Environ, 2011), a chemical transport model, and a detailed emission inventory (Adelman and Omary, 2011). WRF (Skamarock et al., 2008) was used to generate hourly meteorological fields

on three nested domains of 34 vertical layers and horizontal grid sizes of 36, 12, and 4 km. Data for observational nudging on the 4-km domain were from the Meteorological Assimilation Data Ingest System (MADIS) data set, as well as meteorological data collected as part of RoMANS, including data from a 10-m tower at the core site and a radar wind profiler in Estes Park, CO.

A spatial eigenvector analysis of modeled tracer data was used to group various source regions into larger regions that represent transport from that larger region. These identified groups of source regions were then averaged together for each time period and treated as independent variables in a regression model in which the dependent variables are the measured concentrations of the aerosol of interest and the averaged source regions are the independent variables.

All gaseous species show pronounced diurnal variability throughout the year. Typically, minimum concentrations occur during evening hours and maximums in the late afternoon.  $\text{NH}_3$  has the highest or greatest median difference ratio of about 0.65, while  $\text{NO}_x$  and  $\text{NO}_y$  are also very high at about 0.50. The median difference ratio for  $\text{PM}_{10}$  is lower but still high at 0.40.

In some cases use of  $\text{NH}_{x,\text{gas}}$  in the receptor model yielded higher correlations and variance explained than did URG data, suggesting either sources of reduced nitrogen other than ammonia or possibly that the chemiluminescence measurement has a higher precision than the URG measurement. The relative apportionment between sources is approximately the same whether URG or chemiluminescence measurements are used.

Two objectives of the study were to develop an approximate understanding of the relative contributions of ammonia sources in and outside the state of Colorado to measured reduced gaseous ammonia species in RMNP and to assess whether large ammonia emissions in the agricultural area of the midwestern portion of the United States contributed significantly to ammonia in RMNP. In answer to the first question, the analysis suggests that slightly more ammonia measured at RMNP originates from in-state sources. However, within in the uncertainty of the apportionment methodology, it is fair to say that there is about a 50–50 split between in-state and out-of-state sources.

Regarding the second question, it seems pretty clear that very little of measured ammonia at the receptor site had its origins in the Midwest. The model suggests that no more than about 10% of measured ammonia originates from sources east of eastern Colorado (102.3 longitude).

Sources west of Colorado contribute on the order of 30% of measured ammonia, with California contributing on the order of 13%, eastern Utah contributing 10%, and the Snake River valley of southern Idaho 7%.

The systematic correlation between diurnally varying, local easterly winds measured at the receptor site and diurnal cycling of all aerosol species concentrations suggests Front Range transport into the receptor area.

The inability of the WRF modeled winds to faithfully reproduce these systematic diurnal patterns suggests that the receptor model may be underestimating the contribution of Front Range and northeastern Colorado ammonia emissions. With that said, the receptor model suggests that within the state of Colorado, on the average about an equal amount of ammonia is coming from western and central Colorado and the Front Range, including the

Greeley area, at about 10–15%. Northeastern Colorado is estimated to contribute another 4%. The Yampa River valley is estimated to contribute about 5%.

Concentrations of ammonia are highest during the summer months, when the northern Front Range of Colorado and California, along with western and central Colorado and Utah, have the largest contributions. During the spring season, the Front Range, central Colorado, the Snake River valley, and Utah contribute most of the ammonia, while during the fall season, the Front Range plus northeastern Colorado are the largest contributors to ammonia, with California and western and central Colorado also contributing significantly. The winter season corresponds to the lowest measured concentrations, and source regions are primarily more local, but Utah and Arizona sources contribute at times.

## Acknowledgment

This work was funded by the National Park Service under contract H2370094000. The assumptions, findings, conclusions, judgments, and views presented herein are those of the authors and should not be interpreted as necessarily representing the National Park Service policies.

## References

- Adelman, Z., and M. Omary. 2011. *Emissions Modeling Final Report—Developing 2009 Emissions for the NPS-ARD RoMANS Study, Phase 2*. Chapel Hill, NC: Institute for the Environment, University of North Carolina.
- Bai, H.L., and H.Y. Wen. 2000. Performance of the annular denuder system with different arrangements for  $\text{HNO}_3$  and  $\text{HNO}_2$  measurements in Taiwan. *J. Air Waste Manage. Assoc.* 50(1): 125–30. doi:10.1080/10473289.2000.10463991
- Baron, J.S., H.M. Rueth, A.N. Wolfe, K.R. Nydick, E.J. Allstott, J.T. Minear, and B. Moraska. 2000. Ecosystem responses to nitrogen deposition in the Colorado Front Range. *Ecosystems* 3:352–68. doi:10.1007/s100210000032
- Baron, J.S., T.C. Driscoll, J.L. Stoddard, and E.E. Richer. 2011. Empirical critical loads of atmospheric nitrogen deposition for nutrient enrichment and acidification of sensitive U.S. lakes. *BioScience* 61(8): 602–13. doi:10.1525/bio.2011.61.8.6
- Blett, T., and K. Morris. 2004. *Nitrogen Deposition: Issues and effects in Rocky Mountain National Park*. Technical background document. <http://www.cdph.state.co.us/ap/rmnp/noxtech.pdf>
- Burns, D.A. 2003. Atmospheric nitrogen deposition in the Rocky Mountains of Colorado and southern Wyoming—A review and new analysis of past study results. *Atmos. Environ.* 37:921–32. doi:10.1016/S1352-2310(02)00993-7
- Campbell, D.H., J.S. Baron, K.A. Tonnessen, P.D. Brooks, and P.F. Schuster. 2000. Controls on nitrogen flux in alpine/subalpine watersheds of Colorado. *Water Resources Res.* 36:37–47. doi:10.1029/1999WR900283
- Campbell, D.H., C. Kendall, C.C.Y. Chang, S.R. Silva, and K.A. Tonnessen. 2002. Pathways for nitrate release from an alpine watershed: Determination using delta N-15 and delta O-18. *Water Resources Res.* 38. doi:10.1029/2001WR00294
- CASTNET. 2010. *Annual Report*. Washington, DC: U.S. Environmental Protection Agency.
- Demerjian, K.L. 2000. A review of national monitoring networks in North America. *Atmos. Environ.* 34(12–14): 1861–84. doi:10.1016/S1352-2310(99)00452-5
- Dudhia, J. 1996. A multi-layer soil temperature model for MM5. In *Proceedings of the 6th PSU/NCAR Mesoscale Model Users' Workshop*. Boulder, CO: National Center for Atmospheric Research: 49–50.
- Dunlea, E.J., S.C. Herndon, D.D. Nelson, R.M. Volkamer, F. San Martini, P.M. Sheehy, M.S. Zahniser, J.H. Shorter, J.C. Wormhoudt, B.K. Lamb, E.J.

- Allwine, J.S. Gaffney, N.A. Marley, M. Grutter, C. Marquez, S. Blanco, B. Cardenas, A. Retama, C.R.R. Villegas, C.E. Kolb, L.T. Molina, and M.J. Molina. 2007. Evaluation of nitrogen dioxide chemiluminescence monitors in a polluted urban environment. *Atmos. Chem. Phys.* 7(10): 2691–704. doi:10.5194/acp-7-2691-2007
- ENVIRON. 2011. *CAMx User's Guide Version 5.30*. Novato, CA: ENVIRON International Corp.
- Fehsenfeld, F.C., R.R. Dickerson, G. Hubler, W.T. Luke, L.J. Nunnermacker, E.J. Williams, J.M. Roberts, J.G. Calvert, C.M. Curran, A.C. Delany, C.S. Eubank, D.W. Fahey, A. Fried, B.W. Gandrud, A.O. Langford, P.C. Murphy, R.B. Norton, K.E. Pickering, and B.A. Ridley. 1987. A ground-based inter-comparison of NO, NO<sub>x</sub>, and NO<sub>y</sub> measurement techniques. *J. Geophys. Res.* Atmos. 92(D12): 14710–22. doi:10.1029/JD092iD12p14710
- Fontijn, A., A.J. Sabadell, and R.J. Ronco. 1970. Homogeneous chemiluminescent measurement of nitric oxide with ozone—Implications for continuous selective monitoring of gaseous pollutants. *Anal. Chem.* 42(6). doi:10.1021/ac60288a034
- Galloway, J.N., G.E. Likens, W.C. Keene, and J.M. Miller. 1982. The composition of precipitation in remote areas of the world. *J. Geophys. Res.* 87:8771–76. doi:10.1029/JC087iC11p08771
- Galloway, J.N., W.H. Schlesinger, H. Levy, A. Michaels, and J.L. Schnoor. 1995. Nitrogen fixation: Atmospheric enhancement—Environmental response. *Global Biogeochem. Cycles* 9:235–52. doi:10.1029/95GB00158
- Golub, G.H., and C. Reinsch. 1970. Singular value decomposition and least squares solutions. *Numer. Math.* 14:403–20. doi:10.1007/BF02163027
- Hand, J.L., S.A. Copeland, D.E. Day, A.M. Dillner, H. Indresand, W.C. Malm, C.E. McDade, C.T. Moore, Jr., M.L. Pitchford, B.A. Schichtel, and J.G. Watson. 2011. *Spatial and seasonal patterns and temporal variability of haze and its constituents in the United States*. Fort Collins, CO: Cooperative Institute for Research in the Atmosphere, Colorado State University.
- Hedin, L.O., J.J. Armesto, and A.H. Johnson. 1995. Patterns of nutrient loss from unpolluted, old-growth temperate forests: Evaluation of biogeochemical theory. *Ecology* 76:493–509. doi:10.2307/1941208
- Hong, S.-Y., and S.-W. Kim. 2008. Stable boundary layer mixing in a vertical diffusion scheme. In *Proc. Ninth Annual WRF User's Workshop*. Boulder, CO: National Center for Atmospheric Research. <http://www.mmm.ucar.edu/wrf/users/workshops/WS2008/abstracts/3-03.pdf>
- Hong, S.-Y., Y. Noh, and J. Dudhia. 2006. A new vertical diffusion package with explicit treatment of entrainment processes. *Monthly Weather Rev.* 134:2318–41. doi:10.1175/MWR3199.1
- Kain, J.S. 2004. The Kain-Fritsch convective parameterization: An update. *J. Appl. Meteorol.* 43:170–81. doi:10.1175/1520-0450(2004)043<0170:TKCPAU>2.0.CO;2
- Kain, J.S., and J.M. Fritsch. 1993. Convective parameterization for mesoscale models: The Kain-Fritsch scheme. In *The Representation of Cumulus Convection in Numerical Models*, ed. K.A. Emanuel and D.J. Raymond, 165–170. Boston, MA: American Meteorological Society.
- Lehmann, C.M.B., V.C. Bowersox, and S.M. Larson. 2005. Spatial and temporal trends of precipitation chemistry in the United States. *Environ. Pollut.* 135:347–61. doi:10.1016/j.envpol.2004.11.016
- Malm, W.C., D.E. Day, S. Kreidenweis, J.L. Collett Jr., C.M. Carrico, G.R. McMeeking, T. Lee, J. Carrillo, and B.A. Schichtel. 2005. Hygroscopic properties of an organic-laden aerosol. *Atmos. Environ.* 39:4969–82. doi:10.1016/j.atmosenv.2005.05.014
- Mesinger, F., G. DiMego, E. Kalnay, K. Mitchell, P.C. Shafran, W. Ebisuzaki, D. Jovic, J. Woollen, E. Rogers, E.H. Berberry, M.B. Ek, Y. Fan, R. Grumbine, W. Higgins, H. Li, Y. Lin, G. Manikin, D.D. Parrish, and W. Shi. 2006. North American regional reanalysis. *Bull. Am. Meteorol. Soc.* 87:343–60. doi:10.1175/BAMS-87-3-343
- Mlawer, E.J., S.J. Taubman, P.D. Brown, M.J. Iacono, and S.A. Clough. 1997. Radiative transfer for inhomogeneous atmospheres: RRTM, a validated correlated-k model for the longwave. *J. Geophys. Res.* 102(14):16663–82. doi:10.1029/97JD00237
- North American Regional Reanalysis. 2009. Home page. <http://www.emc.ncep.noaa.gov/mmb/rreanl/index.html> (accessed 2009).
- Parrish, D.D., and F.C. Fehsenfeld. 2000. Methods for gas-phase measurements of ozone, ozone precursors and aerosol precursors. *Atmos. Environ.* 34(12–14): 1921–57. doi:10.1016/S1352-2310(99)00454-9
- Rueth, H.M., and J.S. Baron. 2002. Differences in Englemann spruce forest biogeochemistry east and west of the Continental Divide. *Ecosystems* 5:45–57. doi:10.1007/s10021-001-0054-8
- Seinfeld, J.H., and S.N. Pandis. 1998. *Atmospheric Chemistry and Physics: From Air Pollution to Climate Change*. New York, NY: John Wiley.
- Skamarock, W.C., J.B. Klemp, J. Dudhia, D. Gill, D. Barker, M.G. Duda, X.Y. Huang, W. Wang, and J.G. Powers. 2008. A Description of the Advanced Research WRF Version 3. NCAR Technical Note, NCAR/TN-475+STR. Boulder, CO: National Center for Atmospheric Research (NCAR).
- Williams, E.J., K. Baumann, J.M. Roberts, S.B. Bertman, R.B. Norton, F.C. Fehsenfeld, S.R. Springston, L.J. Nunnermacker, L. Newman, K. Olszyna, J. Meagher, B. Hartsell, E. Edgerton, J.R. Pearson, and M.O. Rodgers. 1998. Intercomparison of ground-based NO<sub>y</sub> measurement techniques. *J. Geophys. Res. Atmos.* 103(D17): 22261–80. doi:10.1029/98JD00074

## About the Authors

**William C. Malm** is a senior research scientist at the Cooperative Institute for Research in the Atmosphere, Colorado State University, Fort Collins, CO.

**Bret A. Schichtel**, **Michael G. Barna**, and **Kristi A. Gebhart** are physical scientists for the National Park Service, Air Resources Division, Fort Collins, CO.

**Jeffrey L. Collett, Jr.**, and **Sonia M. Kreidenweis** are professors and **Anthony J. Prenni** is a research scientist at the Department of Atmospheric Science, Colorado State University, Fort Collins, CO. **Katherine B. Benedict** was a postdoctoral research assistant at the Department of Atmospheric Science, Colorado State University, at the time of writing and is currently at the University of California, Davis.

**Christian M. Carrico** is a senior air quality scientist and **Marco A. Rodriguez** is an air quality scientist for AECOM, Inc., Fort Collins, CO.